A sponsored supplement to *Science*

The future of antibody engineering today:

Designing custom antibody tools for life science applications

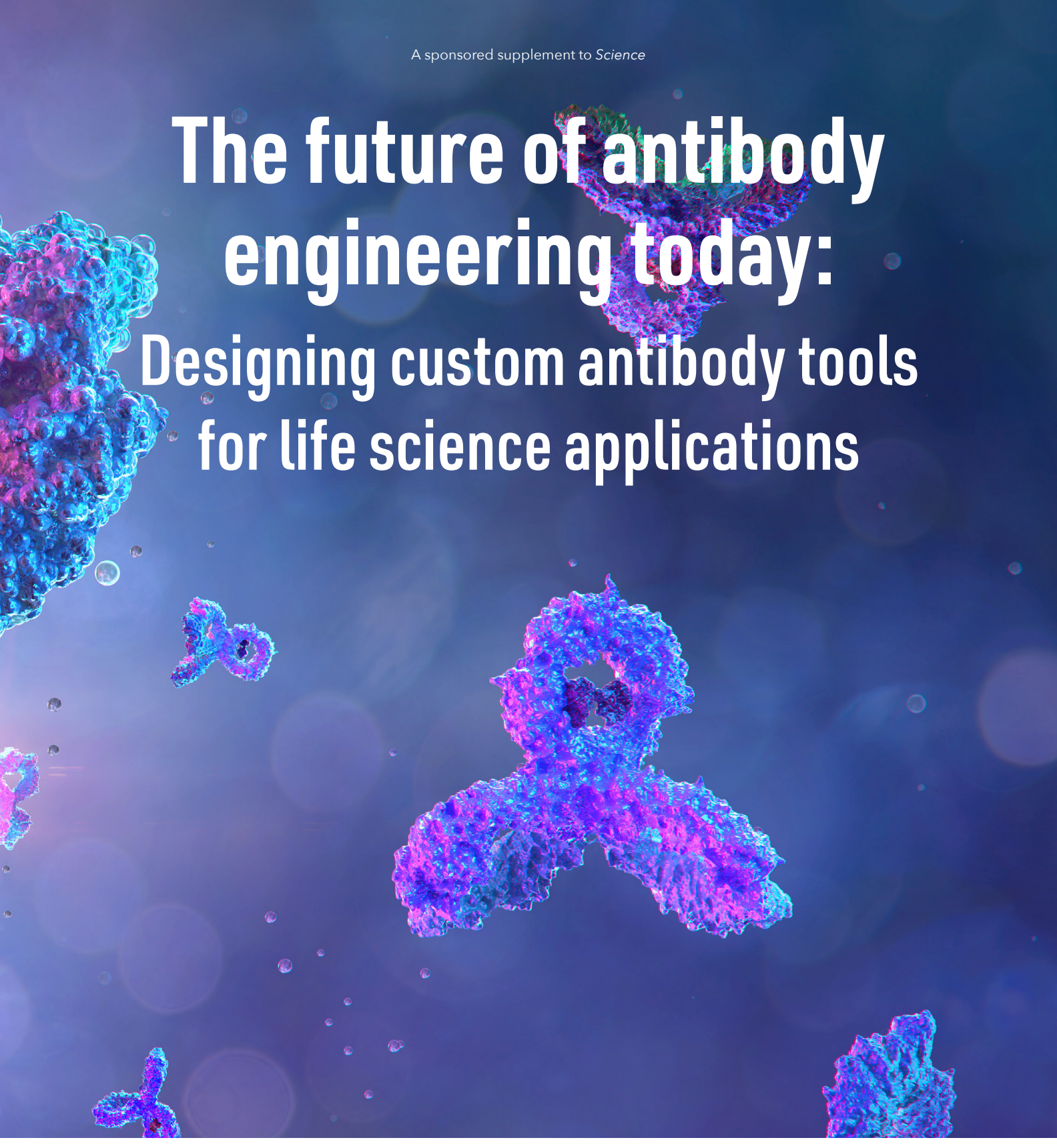

Sponsored by

FORTIS LIFE SCIENCES

Produced by the *Science*/AAAS Custom Publishing Office

Science | AAAS

Table of Contents

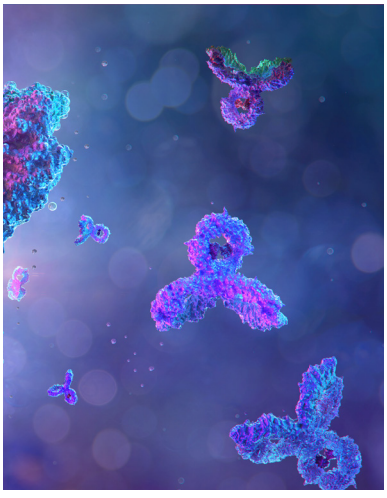

About the Cover:
Artist 3D rendition of antibodies against SARS-CoV-2 virus. © CORONA BOREALIS STUDIO/SHUTTERSTOCK.COM

This supplement was produced by the *Science*/AAAS Custom Publishing Office and sponsored by Fortis Life Sciences.

The original content articles that appear in this supplement have not been peer-reviewed nor have they been assessed by *Science*.

Editor: Jackie Oberst, Ph.D.
Proofreader/Copyeditor: Bob French
Designer: JD Huntsinger

ROGER GONCALVES,
ASSOCIATE SALES DIRECTOR
Custom Publishing
Europe, Middle East, and India
rgoncalves@science-int.co.uk
+41-43-243-1358

16 September 2022

Introductions

2 Antibody engineering: Limitless options and opportunities
Jackie Oberst, Ph.D.
Science/AAAS

3 Fortis. For You.

Research Articles

4 BRD4 methylation by the methyltransferase SETD6 regulates selective transcription to control mRNA translation
Zlata Vershinin, Michal Feldman, Thilo Werner *et al.*

17 Cancer cells use self-inflicted DNA breaks to evade growth limits imposed by genotoxic stress
Brian D. Larsen, Jan Benada, Philip Yuk Kwong Yung *et al.*

Original Content from Sponsor

25 Ten reasons to select Fortis Life Sciences for your custom monoclonal antibody project

26 Raising the bar for biomarkers and early diagnostics in neurodegenerative disease
Lori Kobayashi

28 Reinvigorating the immune system to attack cancer cells using highly specific antibodies
Bijan Etemad-Gilbertson, Ph.D.

29 Setting high standards for antibody production using nucleosomes
Michael-Christopher Keogh, Ph.D.

31 Antibody applications across science and medicine

Antibody engineering: Limitless options and opportunities

Remarkable developments in antibody research and its therapeutic applications have occurred over the last couple of decades. Thanks to molecular biology, it is possible to manipulate the specificities and activities of antibody structures in virtually limitless ways for both basic research and clinical settings. From the development of hybridomas in the 1970s, which created immortalized antibodies, to the latest advances in phage display and genetic engineering techniques such as single B-cell cultures, scientists have created highly specific recombinant antibodies with enhanced immunoprotective abilities, such as engaging immune effector functions and promoting more efficient tumor and tissue penetration.

Current antibody drugs have fewer side effects than their predecessors and have become the predominant class of new drugs developed for treating various human diseases, including many cancers, autoimmune, metabolic, and infectious diseases. In 2018, eight of the top 10 bestselling drugs worldwide were biologics. The global therapeutic monoclonal antibody market is expected to generate revenue of USD $300 billion by 2025.

Similarly, there are many flavors of custom antibodies that can be used in the lab. Phosphospecific antibodies, polyclonal or monoclonal antibodies that detect the phosphorylation site of a target protein, are used to suss out the complex cell signaling involved in apoptosis, cell growth, and cancer. Anti-idiotypic antibodies recognize the idiotypic or variable region of another antibody and play a role in immunogenicity assays and pharmacokinetic/pharmacodynamics (PK/PD) studies. Bispecific antibodies contain two different antigen binding sites and can be used in diagnostics.

Within the pages of this supplement, you will find recent research articles that show how antibody engineering has impacted cancer and epigenetics. Also included are customer testimonials that examine the impact specialized antibodies have had on their respective fields of neurology, oncology, and cell biology. Lastly you will discover a primer on polyclonal and monoclonal antibodies that contains tips on choosing the best type of antibody for your research. We hope you find this supplement useful. Perhaps your research will unearth a new technique in antibody engineering or create the latest life-saving drug.

Jackie Oberst, Ph.D.
Custom Publishing Office
Science/AAAS

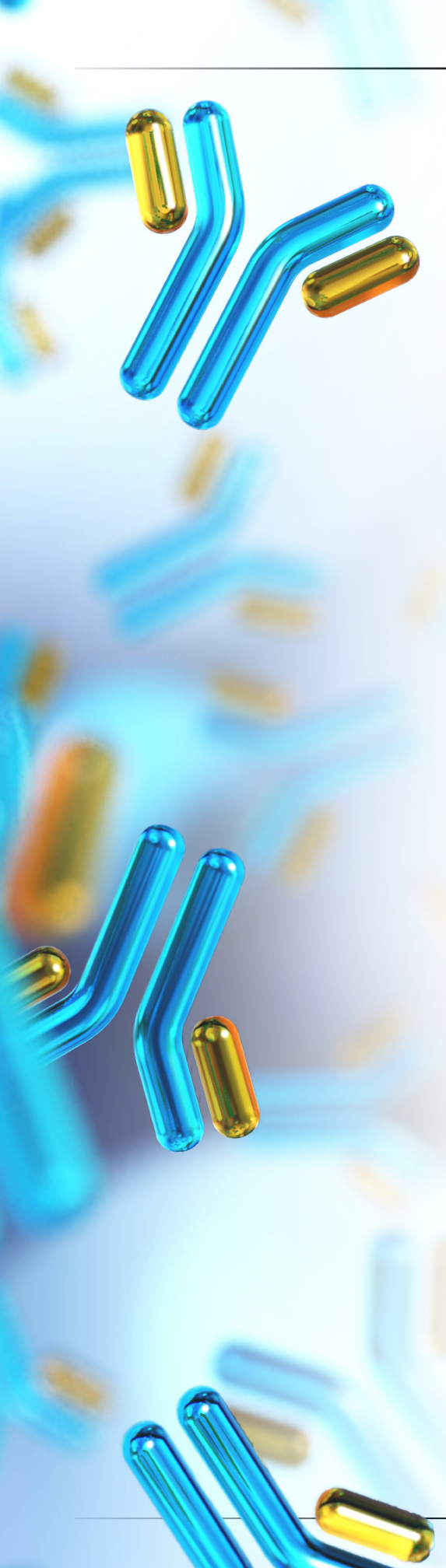

Fortis. For You.

Pursuit of a healthier world starts here.

Fortis Life Sciences offers world-class reagents, tools, materials, and custom services coupled with a best-in-class customer experience for diagnostic manufacturers, biopharma scientists, and researchers. We understand the impact that scientific discovery has on society and how it affects people and human health. Therefore, we think about the effect your work has on the world every single day.

Antibodies are a crucial reagent used in R&D, diagnostics, and therapeutics—from ELISA, flow cytometry, and immunohistochemistry to immunotherapies and lateral flow assays. Having a fit-for-purpose antibody that meets your specific requirements and is validated to work in your desired application ensures project success.

In this eBook, you'll learn about diverse applications for custom antibodies in R&D and drug discovery. You'll hear from scientists who selected custom antibody development in their biopharma workflow. And we will highlight some recent advances in cancer biology and epigenetics that were only possible because of custom antibodies developed to recognize novel targets.

Custom Antibody Services from Fortis Life Sciences

Not all antibodies are created equal. The way your custom antibodies are produced can make all the difference to your success.

At Fortis, we are 100% vertically integrated from antigen to antibody, giving us complete supply chain control and de-risking the process. We manage the entire production and quality control process from start to finish at our in-house facility to provide you with high levels of project customization and scalability. This comprehensive service gives our customers peace of mind and confidence in our products. Our custom antibody services include:

- Custom Recombinant Monoclonal Antibodies
- Custom Polyclonal Antibodies
- Custom Nanobody Discovery
- Antibody Conjugation
- Bulk Antisera

And because we design and manufacture all antibodies in-house, the entire workflow can be customized to meet your needs. Learn more about how we can be an extension of your lab:

https://www.fortislife.com/custom-antibody-production-services

FORTIS
LIFE SCIENCES

BIOCHEMISTRY

BRD4 methylation by the methyltransferase SETD6 regulates selective transcription to control mRNA translation

Zlata Vershinin[1,2], Michal Feldman[1,2], Thilo Werner[3], Lital Estrella Weil[1,2], Margarita Kublanovsky[1,2], Elina Abaev-Schneiderman[1,2], Menachem Sklarz[2], Enid Y. N. Lam[4], Khawla Alasad[2,5], Sarah Picaud[6], Barak Rotblat[2,5], Ruth A. McAdam[7], Vered Chalifa-Caspi[2], Marcus Bantscheff[3], Trevor Chapman[7], Huw D. Lewis[7], Panagis Filippakopoulos[6], Mark A. Dawson[4], Paola Grandi[3], Rab K. Prinjha[7], Dan Levy[1,2]*

The transcriptional coactivator BRD4 has a fundamental role in transcription regulation and thus became a promising epigenetic therapeutic candidate to target diverse pathologies. However, the regulation of BRD4 by posttranslational modifications has been largely unexplored. Here, we show that BRD4 is methylated on chromatin at lysine-99 by the protein lysine methyltransferase SETD6. BRD4 methylation negatively regulates the expression of genes that are involved in translation and inhibits total mRNA translation in cells. Mechanistically, we provide evidence that supports a model where BRD4 methylation by SETD6 does not have a direct role in the association with acetylated histone H4 at chromatin. However, this methylation specifically determines the recruitment of the transcription factor E2F1 to selected target genes that are involved in mRNA translation. Together, our findings reveal a previously unknown molecular mechanism for BRD4 methylation–dependent gene-specific targeting, which may serve as a new direction for the development of therapeutic applications.

INTRODUCTION

The transcription regulator BRD4 is a member of the bromodomain and extraterminal domain (BET) protein family. BRD4 contains two conserved bromodomains (*1*, *2*) that specifically recognize acetylated lysine residues on histone and non-histone proteins (*3*–*7*). This binding is known to regulate transcription of target genes involved in a wide range of biological processes and diseases (*3*–*5*, *8*). The critical role of BRD4 in the transcription process marks it as an attractive candidate for pharmacological intervention. BET inhibitors, targeting BRD family members and displacing them from chromatin, were studied extensively in different malignancies in recent years, demonstrating a notable therapeutic potential (*4*, *8*–*16*). However, little is known about their regulation by posttranslational modifications.

Lysine methylation, catalyzed by protein lysine methyltransferases (PKMTs), is emerging as a prominent posttranslation modification that regulates different signaling pathways (*17*–*21*). The monomethyltransferase SET domain–containing protein 6 (SETD6) was originally identified to directly methylate RelA [p65, a subunit of nuclear factor κB (NF-κB) complex] and, thereby, to suppress the activation of NF-κB target genes (*22*). SETD6 was also shown to play an important role in cell cycle regulation, oxidative stress response, WNT signaling, embryonic stem cell self-renewal, nuclear hormone receptor signaling, and cellular proliferation in several cellular models (*23*–*28*). The fact that BRD4 is tightly linked to the regulation of many of these processes raised the intriguing hypothesis of potential cellular and functional cross-talk between SETD6 and BRD4.

Here, we demonstrate that SETD6 binds and methylates the lysine-99 (K99) residue of BRD4 on chromatin. RNA sequencing (RNA-seq) experiments revealed that BRD4 methylation regulates the expression of genes that are involved in translation and inhibits total mRNA translation in cells. Mechanistically, our data suggest that SETD6-mediated methylation of BRD4 at K99 affects neither the integrity of ribosome complexes nor the interaction of BRD4 with acetylated H4 on chromatin. We provide evidence that supports a model where BRD4, independent of its methylation at K99, is present on chromatin on genes that are involved in translation. Our data rather suggest that BRD4 methylation state on chromatin selectively determines the recruitment of the transcription factor E2F1 to these target genes and, hence, their transcriptional activation.

RESULTS

SETD6 methylates and binds BRD4 in vitro and in cells

To test whether BRD4 is methylated by SETD6 in vitro, we performed a radioactive methylation assay in the presence of truncated His-tagged BRD4 (1-477aa) and GST SETD6 (Fig. 1A). The results suggest that SETD6 methylates BRD4. BRD4 contains two bromodomains, BD1 and BD2 (see diagram in Fig. 2A), and we used these recombinant fragments to initially map the methylation site. As shown in Fig. 1B, our results suggest that SETD6 directly and specifically methylates the BD1 domain, but not BD2. To determine whether BRD4 is methylated while associated with chromatin, we overexpressed Flag BRD4 (1-477aa), together with HA-tagged SETD6 in human embryonic kidney (HEK) 293T cells. The cells were then submitted to chromatin extraction followed by immunoprecipitation using protein-protein

[1]The Shraga Segal Department of Microbiology, Immunology and Genetics, Ben-Gurion University of the Negev, P.O.B. 653, Be'er-Sheva 84105, Israel. [2]National Institute for Biotechnology in the Negev, Ben-Gurion University of the Negev, P.O.B. 653, Be'er-Sheva 84105, Israel. [3]GSK Cellzome GmbH, Functional Genomics R&D, 69117 Heidelberg, Germany. [4]Sir Peter MacCallum Department of Oncology and Centre for Cancer Research, University of Melbourne, Melbourne, Australia. [5]Department of Life Sciences, Ben-Gurion University of the Negev, Be'er-Sheva 84105, Israel. [6]Structural Genomics Consortium, Nuffield Department of Clinical Medicine, University of Oxford, Oxford OX3 7DQ, UK. [7]GSK, Medicines Research Centre, Gunnels Wood Road, Stevenage, Hertfordshire SG1 2NY, UK.
*Corresponding author. Email: ledan@post.bgu.ac.il

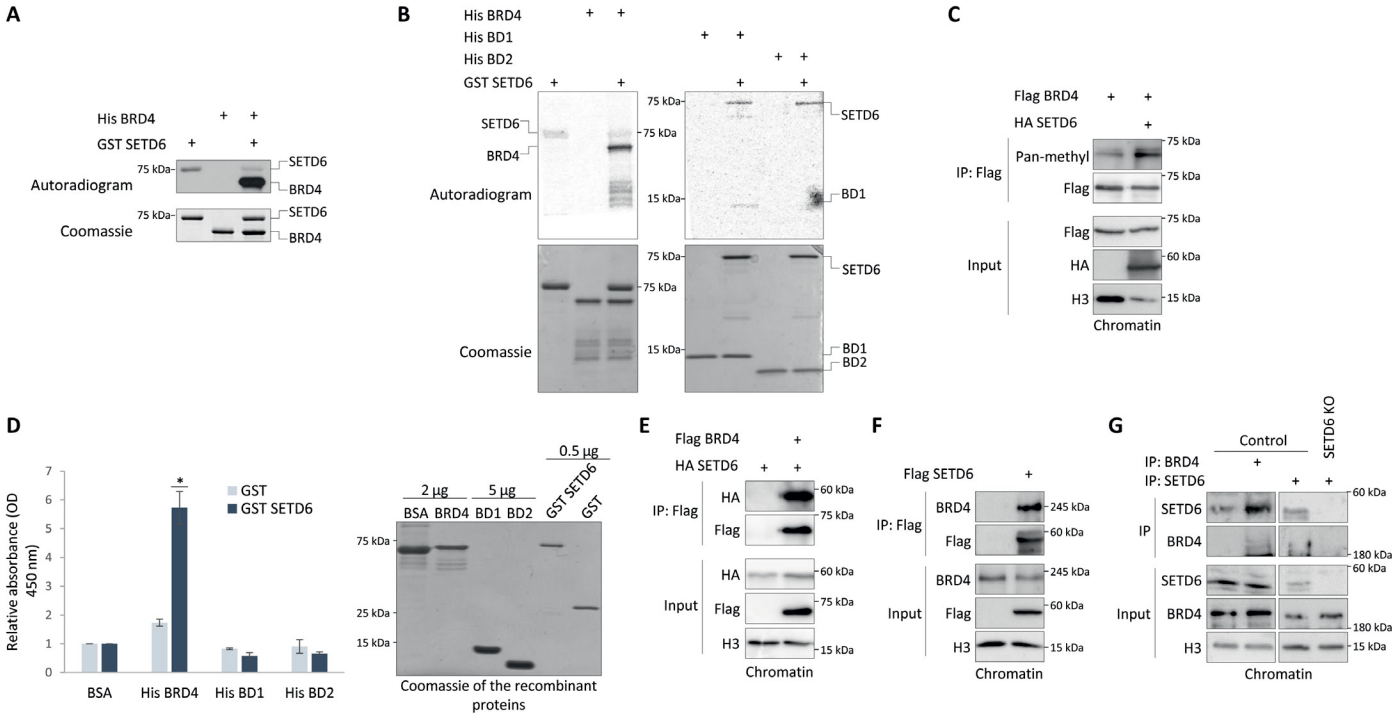

Fig. 1. SETD6 binds and methylates BRD4 in vitro and on chromatin in cells. (**A** and **B**) In vitro methylation of BRD4 by SETD6. Samples were subjected to SDS–polyacrylamide gel electrophoresis (PAGE) followed by exposure to autoradiogram to detect ^{3}H-labeled proteins or Coomassie staining to detect all proteins. (**C**) SETD6 methylates BRD4 in cells. Human embryonic kidney (HEK) 293T wild-type cells were transfected with Flag BRD4 (1-477aa) with or without HA SETD6. Chromatin fractions from HEK293T cells were immunoprecipitated with FLAG-M2 beads, followed by Western blot analysis with indicated antibodies. (**D**) In vitro interaction between SETD6 and BRD4. Enzyme-linked immunosorbent assay (ELISA) was performed with the indicated recombinant proteins. The graph represents relative absorbance normalized to bovine serum albumin (BSA) signal of each condition. Error bars are SD. On the right, Coomassie staining represents all proteins used in this assay. Statistical analysis was performed for three experimental repeats using Student's *t* test. **P* < 0.05. (**E** to **G**) SETD6 binds BRD4 in cells. Chromatin fractions of HEK293T (E) and MDA-MBA-231 (F and G) cells, transfected or not as indicated, were isolated, immunoprecipitated, and submitted to Western blot analysis with the indicated antibodies.

chromatin immunoprecipitation (ChIP) protocol, as previously described (*29*). Western blotting with a pan-methyl antibody revealed that BRD4 methylation level was increased on chromatin in the presence of SETD6 (Fig. 1C).

We next investigated the physical interaction between BRD4 and SETD6. A direct interaction between the proteins was tested in an enzyme-linked immunosorbent assay (ELISA). In these experiments, recombinant His BRD4 (1-477aa), His BD1, His BD2, or bovine serum albumin (BSA) as negative control was immobilized on a 96-well plate, followed by incubation with recombinant glutathione *S*-transferase (GST) SETD6 or GST (Fig. 1D). The results suggest that SETD6 directly binds BRD4, but not through its bromodomains. Co-IP experiments were then performed and showed an interaction in the chromatin fraction between both overexpressed and tagged proteins in HEK293T cells (Fig. 1E), between overexpressed SETD6 and endogenous BRD4 in MDA-MB-231 cells (Fig. 1F), and also between endogenous SETD6 and BRD4 in MDA-MB-231 cells (Fig. 1G). Collectively, our data suggest that SETD6 methylates and binds BRD4 in vitro and in cells directly on chromatin.

SETD6 methylates BRD4 at lysine-99

These findings prompted us to map BRD4 methylation site by SETD6. Using mass spectrometry analysis, we identified mono-methylation on lysine-99 (K99), which is located inside the BD1 domain (Fig. 2A and fig. S1, A and B). Extracted ion chromatograms of the corresponding tryptic peptides showed an incubation time–dependent increase of the mono-methylation in the presence of the cosubstrate *S*-adenosylmethionine (SAM), confirming that site occupancy is dependent on the enzymatic activity of SETD6 (fig. S1, C and D). To validate these findings, we performed an in vitro methylation reaction using recombinant His-Sumo BRD4 wild type and BRD4 K99R proteins as substrates. The methylation signal of the mutant BRD4 K99R was significantly lower compared to BRD4 wild type, suggesting that K99 is the primary methylation site targeted by SETD6 (Fig. 2B). While the mass spectrometry analysis identified only one methylation site, the remaining signal in the BRD4 K99R mutant may suggest that there are additional methylation sites on BRD4. Catalytically inactive SETD6 mutant (Y285A) (*22*, *30*) served as a negative control for the reaction. These results were confirmed in a semi–in vitro methylation assay where immunoprecipitated overexpressed Flag BRD4 wild type or K99R from the chromatin fraction was subjected to an in vitro methylation assay in the presence of recombinant SETD6 (Fig. 2C). To test BRD4 methylation in cells, we generated site- and state-specific antibodies to recognize methylated BRD4 at K99. We used two rabbit polyclonal antibodies, U292 and U293, which were raised against two BRD4 mono-methylated peptides at K99 (see Materials and Methods). Both antibodies could specifically detect methylated BRD4 peptides (1 and 2) in a dose-dependent

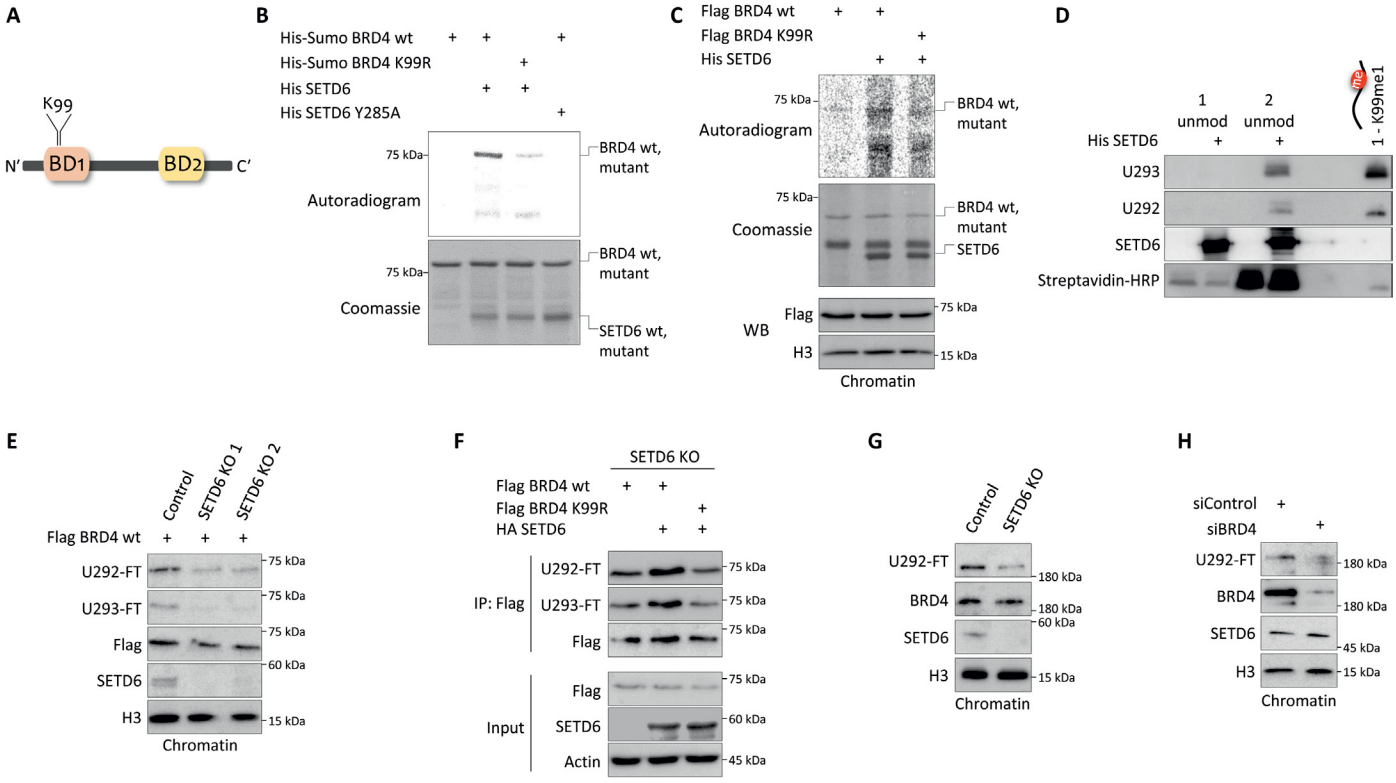

Fig. 2. SETD6 methylates BRD4 at K99. (**A**) Illustration of truncated BRD4 (1-477aa) with identified lysine-99 (K99) as the methylation site by SETD6. (**B**) SETD6 methylates BRD4 at K99 in vitro. In vitro methylation reaction with the indicated recombinant proteins was incubated in the presence of ^{3}H-labeled SAM. Samples were then resolved by SDS-PAGE followed by exposure to autoradiogram detection or Coomassie staining. (**C**) Semi–in vitro methylation assay. Immunoprecipitated Flag-BRD4 from HEK293T SETD6 knockout (KO) cell chromatin fractions were subjected to radioactive in vitro methylation assay. (**D**) In vitro validation of BRD4 K99me1 antibodies (U292 and U293). Unmodified biotin-labeled BRD4 peptides were incubated with or without His SETD6 in the presence of cold *S*-adenosylmethionine (SAM) followed by Western blot (WB) analysis with the indicated antibodies.1-K99me1 peptide served as positive control. (**E** to **H**) Validation of BRD4 K99me1 antibodies (U292-FT and U293-FT) in cells under different experimental conditions. (E) Chromatin fraction of MDA-MB-231 control and CRISPR SETD6 KO cells overexpressing Flag BRD4 wild type (wt). (F) Flag immunoprecipitation of MDA-MB-231 CRISPR SETD6 KO cells overexpressing Flag BRD4 wild type or Flag BRD4 K99R (1-477aa). (G) Chromatin fraction of MDA-MB-231 control and CRISPR SETD6 KO. (H) Chromatin fraction of MDA-MB-231 wild-type cells treated with siRNA control or BRD4 for 48 hours.

manner and not the unmodified or scrambled peptides (fig. S2A). In addition, both antibodies specifically recognized the methylation induced by His SETD6 on peptide 2, but not on peptide 1, suggesting that SETD6 is able to methylate peptide 2, but not peptide 1 (Fig. 2D and Materials and Methods for peptide sequences), most likely due to changes in their conformational recognition following the variation in their amino acid content (see Materials and Methods). K99me1 peptide was used as positive control in this experiment. Furthermore, in an in vitro methylation reaction using recombinant proteins, while cross-reactivity of both antibodies with unmethylated BRD4 was observed, a notable increase in the signal was found when SETD6 was added to the reaction (fig. S2B). In addition, an increase in BRD4 K99 methylation signal was observed using the U293 antibody when Flag BRD4 was immunoprecipitated from MDA-MB-231 cells and incubated with recombinant His SETD6 (fig. S2C). We next used these antibodies to determine whether BRD4 is methylated at K99 in cells. Here, we used U292-FT and U293-FT antibodies, which had been subjected to further affinity purification. Depletion of SETD6 in MDA-MB-231 cells with two independent single-clone guide RNAs (gRNAs) resulted in a decrease in the methylation of Flag BRD4 on chromatin (Fig. 2E). Moreover, in a rescue experiment that was performed in the SETD6 knockout (KO) cells, addition of HA SETD6 increased the methylation of BRD4 wild type but not the K99 mutant (Fig. 2F), suggesting that the methylation of BRD4 at K99 is SETD6 dependent. A substantial reduction in the methylation of endogenous BRD4 was observed in the SETD6 KO cells on chromatin (Fig. 2G). To confirm that the signal in cells is specific to BRD4, endogenous BRD4 was knocked down with small interfering RNA (siRNA), and the level of BRD4 methylation at the chromatin was further assessed with the K99me antibody (U292-FT). As shown in Fig. 2H, silencing of BRD4 correlates with a reduction of its methylation level. Together, these data suggest that SETD6 specifically methylates BRD4 at K99 in vitro and in cells.

SETD6-mediated methylation of BRD4 at K99 regulates the expression of genes involved in mRNA translation

We hypothesized that BRD4 methylation at K99 by SETD6 may serve as a regulatory mechanism to mediate BRD4 function to govern gene expression programs. To address this hypothesis, we designed an RNA-seq experiment using MDA-MB-231 control and SETD6 CRISPR KO or knockdown (KD) cells (Fig. 3A) and MDA-MB-231 cells stably expressing an empty plasmid, Flag BRD4 wild type (1-477aa), or Flag

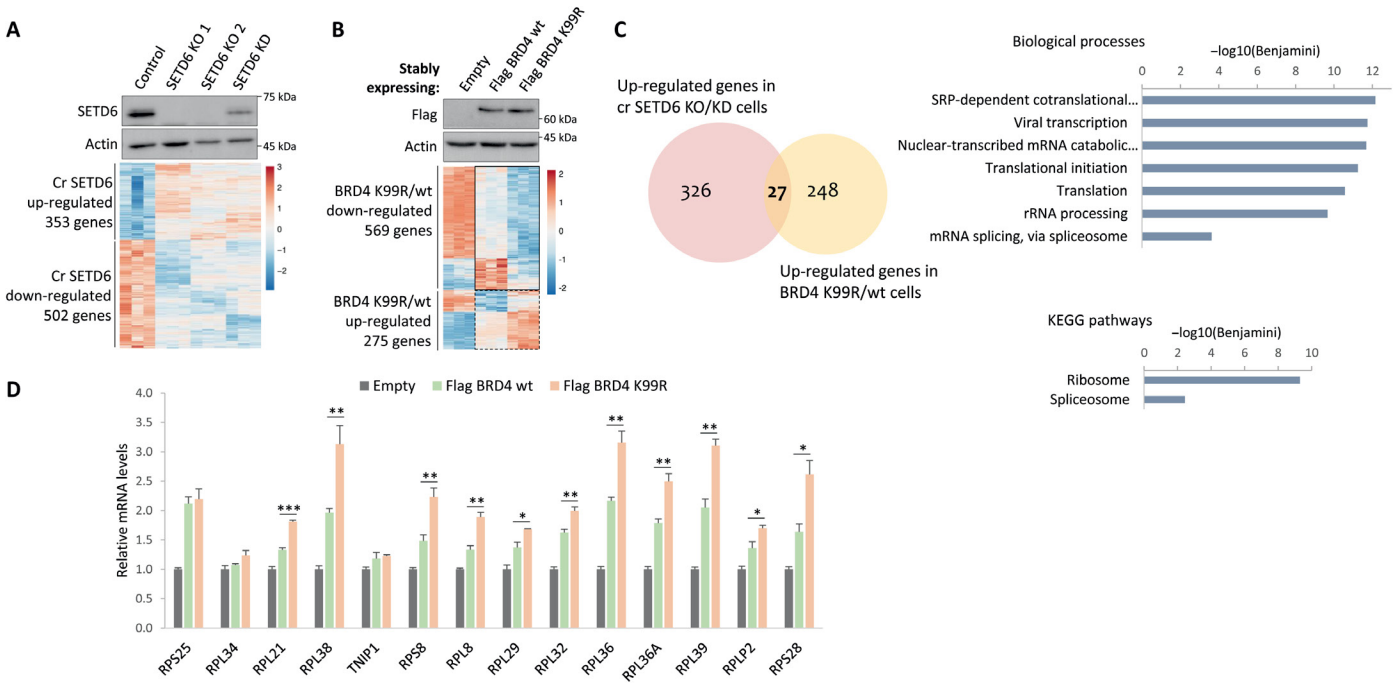

Fig. 3. SETD6-mediated methylation of BRD4 at K99 regulates the expression of genes involved in mRNA translation. (**A** and **B**) MDA-MB-231 (A) CRISPR control and SETD6 KO/KD or (B) stably expressing Flag BRD4 wild-type or Flag BRD4 K99R cells were subjected to Western blot indicating SETD6 (A) or Flag BRD4 protein levels (B) in the cells (top). Bottom: Heatmap of differentially expressed up- and down-regulated genes from RNA-seq in all the indicated cells. Orange and blue colors represent higher and lower expression, respectively. (**C**) Common up-regulated (*27*) CRISPR SETD6 KO/KD–dependent and BRD4 K99R–dependent genes were analyzed using the DAVID database for biological processes and Kyoto Encyclopedia of Genes and Genomes (KEGG) pathways (on the right). Pathways shown are based on the Benjamini-corrected *P* value of <0.05. (**D**) Validation of RNA-seq experiments. mRNA was extracted from MDA-MB-231 cells, and transcript levels were determined by quantitative polymerase chain reaction (qPCR). mRNA levels were normalized to glyceraldehyde-3-phosphate dehydrogenase (GAPDH) and then to empty cells. Error bars are SEM. Statistical analysis was performed for three experimental repeats using one-way ANOVA. **P* < 0.05, ***P* < 0.01, and ****P* < 0.001.

BRD4 K99R mutant (Fig. 3B). Total RNAs were extracted from these cells, and triplicate samples were sent for sequencing. We found 353 up-regulated and 502 down-regulated genes in the CRISPR SETD6 KO/KD cells (Fig. 3A, heatmap). We identified 275 up-regulated and 569 down-regulated genes in the cells stably expressing Flag BRD4 K99R in comparison to Flag BRD4 wild type–expressing cells (Fig. 3B, heatmap). Enrichment testing for biological processes and Kyoto Encyclopedia of Genes and Genomes (KEGG) pathways was then carried out to further explore the link between SETD6 and BRD4 methylation at K99. To do so, we compared the down- and up-regulated genes in the SETD6 KO/KD cells to the cells stably expressing the BRD4 K99R mutant. Both conditions mimic the situation by which BRD4 is not methylated. We found diverse pathways, such as cell-matrix adhesion and focal adhesions in the common 67 down-regulated genes (fig. S3). In the common 27 up-regulated gene analysis, we noticed that mRNA translation and ribosomal RNA (rRNA) processing pathways were significantly up-regulated in cells lacking SETD6 or in the cells stably expressing BRD4 K99R mutant (Fig. 3C). The expression of these specific genes was then validated by quantitative polymerase chain reaction (qPCR). As shown in Fig. 3D, a significant elevation in the expression of these genes was found in cells stably expressing BRD4 K99R, which represents an unmethylated state of BRD4. The fact that also the wild-type BRD4 increases expression of those genes indicates that this might be a dosage effect. Collectively, these experiments suggest that SETD6-mediated methylation of BRD4 at K99 negatively affects the expression of genes involved in mRNA translation.

BRD4 methylation at K99 inhibits translation

We hypothesized that unmethylated BRD4 enhances translation in cells. To test this hypothesis, we measured total protein synthesis using the SUnSET method (*31*). In this approach, puromycin (an analog of aminoacyl transfer RNAs) is incorporated into newly synthesized polypeptide chains, and the resulting proteins are detected by Western blot using anti-puromycin antibody. Protein synthesis was elevated in the SETD6 KO cells (two independent gRNAs) compared to control cells, suggesting that depletion of SETD6 enhances mRNA translation (Fig. 4A). In a rescue experiment in MDA-MB-231 SETD6 KO cells, addition of exogenous HA SETD6 to the cells reduced the total protein synthesis (Fig. 4B), which suggests that this phenomenon is SETD6 dependent. We next measured total protein synthesis in MDA-MB-231 cells stably expressing an empty plasmid, Flag BRD4 wild type, or Flag BRD4 K99R mutant. Consistent with our working hypothesis, we found that the protein synthesis is elevated in BRD4 K99R compared to cells stably expressing BRD4 wild type or empty cells (Fig. 4C). Elevated protein synthesis was also observed in cells overexpressing K99R BRD4 long isoform (Fig. 4D). Having demonstrated that SETD6 regulates protein synthesis in a BRD4-dependent manner, we next asked whether BRD4 interacts with monosomes or polysomes. To this end, we performed

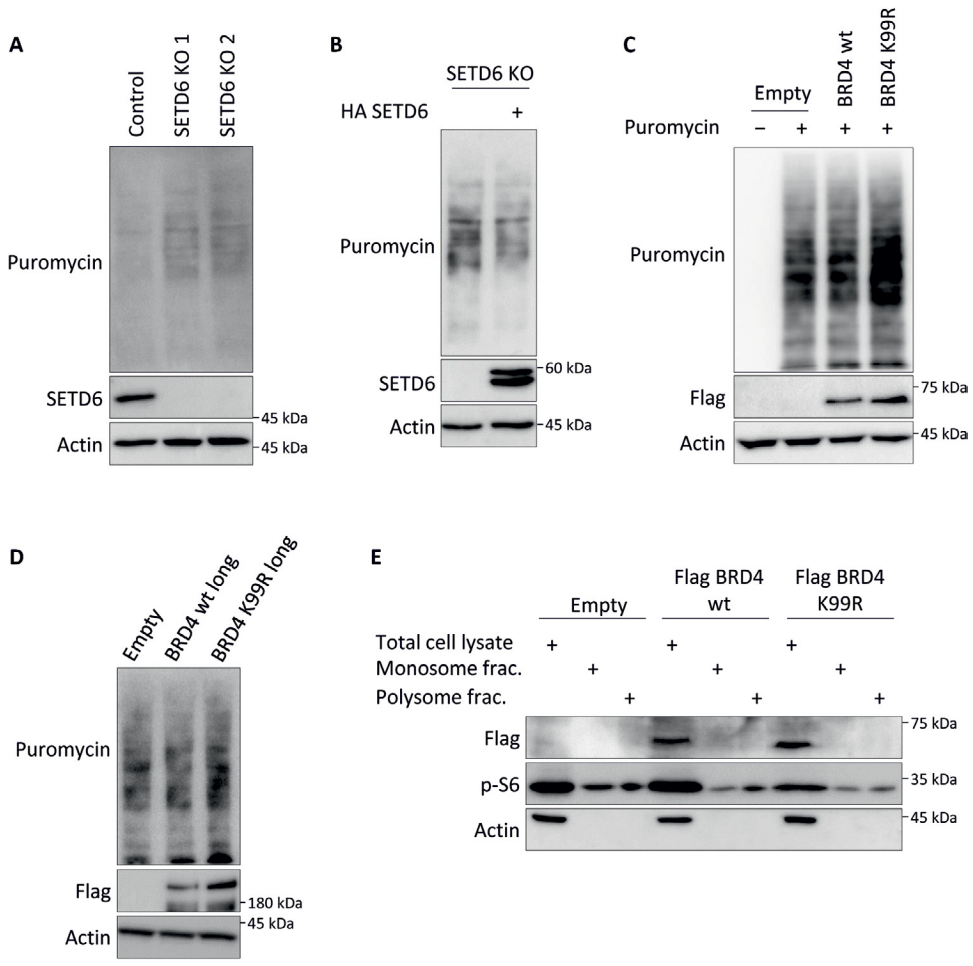

Fig. 4. BRD4 methylation at K99 inhibits translation. (**A** to **D**) Translation assay (SUnSET). (A) MDA-MB-231 control and CRISPR SETD6 KO (two independent gRNAs) cells. (B) MDA-MB-231 CRISPR SETD6 KO cells with or without overexpressed HA SETD6. (C) MDA-MB-231 cells stably expressing empty plasmid, Flag BRD4 wild type, or Flag BRD4 K99R (1-477aa). (D) MDA-MB-231 wild-type cells overexpressing empty plasmid, Flag BRD4 wild type, or Flag BRD4 K99R (long isoform). Cells were incubated with puromycin and then cell extracts were submitted to Western blot to detect protein synthesis using anti-puromycin antibody. (**E**) Polysome profiling. Monosome and polysome fractions were extracted from MDA-MB-231 cells stably expressing empty plasmid, Flag BRD4 wild type, or Flag BRD4 K99R (1-477aa). The fractions and total cell lysates, served as control, were submitted to Western blot analysis with anti-Flag antibody. Actin served as loading control. Phosphorylated S6 (p-S6) served as control for polysome profiling method.

a polysome profiling of cells stably expressing an empty plasmid, Flag BRD4 wild type, or Flag BRD4 K99R. Total cell lysates from these cells and the monosome and polysome fractions were analyzed by Western blot (Fig. 4E). Our results suggest that BRD4 wild type or BRD4 K99R mutant is not part of the monosome or polysome fractions. These results support the observation that the translation regulation by SETD6-mediated methylation of BRD4 at K99 is carried out by controlling the transcription of genes that are then involved in translation.

BRD4 methylation at K99 does not regulate the interaction with acetylated H4 at chromatin

The bromodomains of BRD4 specifically recognize and bind acetylated lysine residues of targeted histone and non-histone proteins (*3*–*7*). Having demonstrated that SETD6 methylates BRD4 at K99, within the BD1 domain, raises the intriguing hypothesis that BRD4 methylation regulates its association with the chromatin and specifically with acetylated histones. To address this hypothesis, we tested whether BRD4 wild type binds acetylated H4 differently than BRD4 K99R in a co-IP experiment using a specific validated antibody that recognizes a tetra-acetylated histone H4 at lysines K5, K8, K12, and K16 (*32*, *33*). To observe a specific signal from this antibody, the addition of the deacetylase inhibitor trichostatin A (TSA) was required to increase global acetylation levels. As expected, without TSA treatment, we could not detect interaction between BRD4 and the tetra-acetylated H4 (Fig. 5A, second lane). Treatment with TSA led to a specific interaction of BRD4 with the tetra-acetylated H4. However, we could not see any difference between wild-type BRD4 and the K99R mutant in their ability to bind tetra-acetylated H4 (Fig. 5A, two lanes on the right), which was not the case for the BRD4 N140F mutant, known for its inability to bind the tetra-acetylated H4 (fig. S4) (*34*). Furthermore, similar binding of tetra-acetylated H4 to endogenous BRD4 was observed in both control and SETD6 KO MDA-MB-231 cells when BRD4 was immunoprecipitated (Fig. 5B).

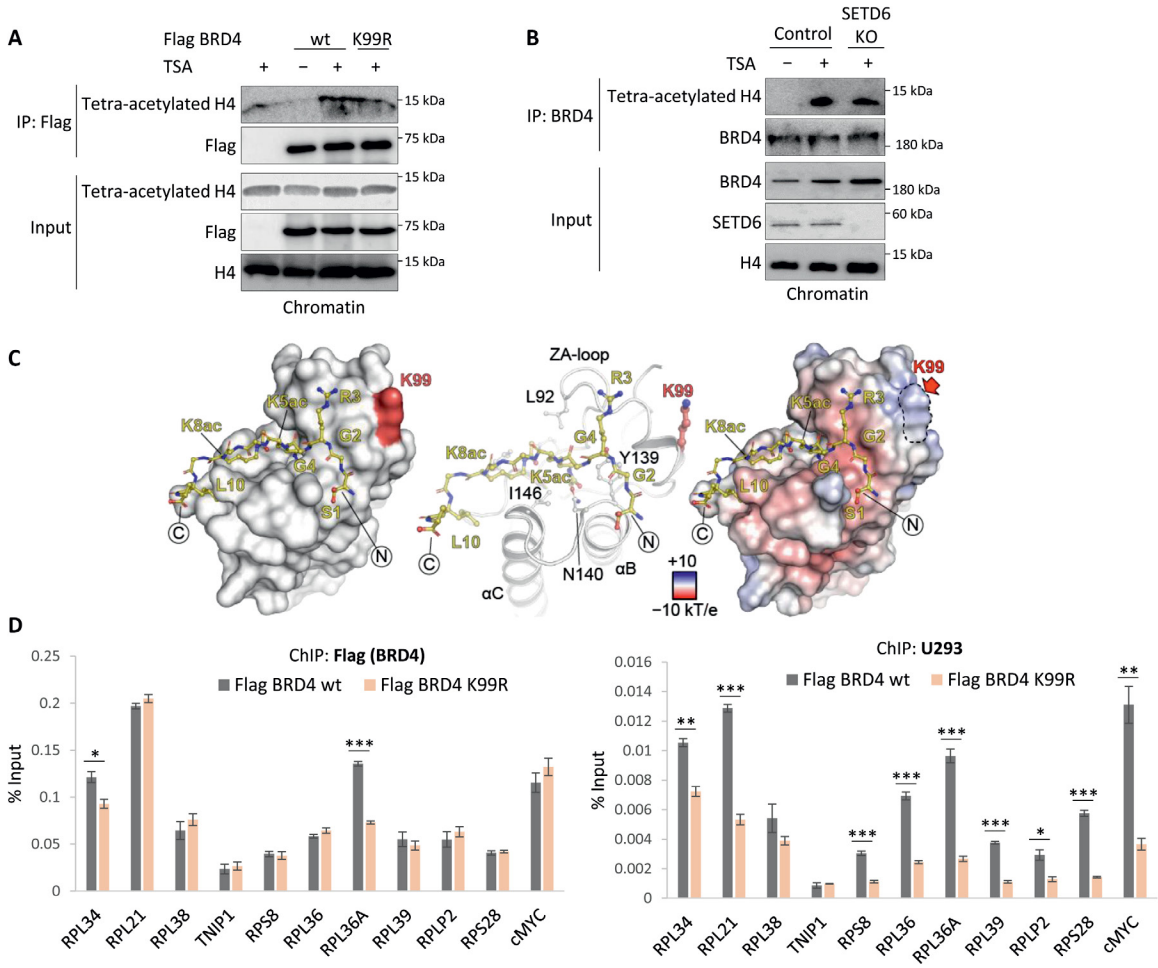

Fig. 5. BRD4 K99me does not affect its binding to acetylated H4. (**A** and **B**) MDA-MB-231 wild-type cells were transfected as indicated and treated with TSA for 4 hours. Chromatin fractions were immunoprecipitated with indicated antibodies, followed by Western blot analysis with anti–tetra-acetylated H4 antibody. (**C**) Left: Topology of the H4K5ac/K8ac (H4 residues 1 to 11) peptide binding to BRD4/BD1. The peptide termini are annotated and the location of K99 is highlighted in red [Protein Data Bank (PDB) ID: 3UVW (*34*)]. Middle: Crystal structure of the complex of BRD4/BD1 with an H4 (1 to 11) K5ac/K8ac peptide (PDB: 3UVW) shown in ribbon and stick representation. Residues that initiate contact are annotated and K99 is shown in red (same orientation as on the left). Right: Binding of H4 (1 to 11) K5ac/K8ac onto the surface of BRD4/BD1. Protein charge distribution is plotted on the surface of BRD4/BD1, highlighting the extensive electrostatic nature of the interaction. Location of K99 is highlighted in red. (**D**) ChIP assay for MDA-MB-231 wild-type cells overexpressing Flag BRD4 wild type or Flag BRD4 K99R (1-477aa) using FLAG-M2 (left) or U293 antibody (right). Graphs show percent input of the quantified DNA. Error bars are SEM. Statistical analysis was performed for three experimental repeats using Student's *t* test. $^{*}P < 0.05$, $^{**}P < 0.01$, and $^{***}P < 0.001$.

To support these observations, analysis of the available structural data in the model of BRD4/BD1 bound to H4K5ac/K8ac showed that there is no direct interaction between any of the histone peptide residues and K99, which is located behind the ZA loop (Fig. 5C). While we cannot rule out that methylation of this site would potentially affect the surface properties of the protein, our cellular data support a model where Kac recognition is not directly affected by K99me. On the molecular level, ChIP experiments (Fig. 5D) for Flag BRD4 wild type and K99R mutant confirmed that both unmethylated and methylated BRD4 (Fig. 5D, right, U293 antibody) are present at chromatin on most of the different genes that are involved in translation that were tested. From this set of experiments, we concluded that the methylation of BRD4 at K99 does not affect the overall recognition and binding to acetylated H4 at chromatin.

BRD4 methylation at K99 controls a selective binding to E2F1 to regulate the transcription of genes that are involved in mRNA translation

Our results so far suggest that SETD6 methylates BRD4 at K99 to regulate the expression of ribosomal target genes and total mRNA translation. We also found that BRD4 methylation does not have a direct role in the assembly of the ribosome complex or in the association with acetylated histone H4 through its bromodomains. We next wanted to understand the underlying mechanism by which SETD6 and the methylation of BRD4 at K99 regulate mRNA translation. To do so, we performed a ChIP-X enrichment analysis (ChEA), which is a gene set enrichment analysis tool to identify a putative binding of transcription factors to a given set of target genes based on published data such as ChIP-chip, ChIP-seq, and ChIP-PET experiments (*35*). We performed the ChEA analysis on the set of

genes that were up-regulated in the BRD4 K99R RNA-seq results shown in Fig. 3B, which displayed an enrichment in processes linked to translation regulation. Of the 275 up-regulated genes, the ChEA analysis identified a significant enrichment (adjusted *P* value of 2.1×0^{-7}) for the transcription factor E2F1 in 100 of them (Fig. 6A). This finding, together with previous reports showing that E2F1 regulates translation (*36*–*38*), implies that methylation of BRD4 at K99 orchestrates a selective binding to E2F1 to regulate transcription of genes involved in mRNA translation. To address this hypothesis, we first performed a translation assay using the SUnSET method and found that in the presence of overexpressed E2F1 in MDA-MB-231 cells, there is an increase in mRNA translation in a dose-dependent manner (fig. S5A). We then performed an ELISA to test for a direct interaction between E2F1 and BRD4 and to determine whether the methylation of BRD4 by SETD6 attenuates this interaction. Our results indicate that BRD4 binds E2F1 and that this interaction is reduced when BRD4 is methylated after the addition of recombinant SETD6 (Fig. 6B). Increased E2F1 binding was observed when BRD4 was incubated with the catalytically inactive SETD6 Y285A, confirming that this phenomenon is methylation dependent in vitro (fig. S5B, and parallel Coomassie stains for the recombinant proteins used in the reaction in fig. S5C). To test whether methylation of BRD4 selectively regulates the interaction with E2F1 in cells, we immunoprecipitated Flag BRD4 in control and SETD6 KO cells. Consistent with our working model, overexpressed E2F1 binds methylated BRD4 in the control cells; however, a stronger interaction was observed in SETD6 KO cells where BRD4 is not methylated (Fig. 6C). Moreover, in a rescue experiment, we found that overexpression of HA SETD6 in the SETD6 KO cells attenuates the interaction between the overexpressed long isoform of BRD4 and endogenous E2F1 (Fig. 6D). These results further support that BRD4 methylation at K99 selectively regulates the binding of E2F1 to specific target genes. In a ChIP experiment, we found a significant enrichment for binding of Flag E2F1 to target genes involved in translation (RNA-seq; Fig. 3, A to C) in cells overexpressing BRD4 K99R compared to wild-type cells (Fig. 6E). E2F1 enrichment correlates well with a significant increase in the transcription of most of the target genes that were tested in cells that express BRD4 K99R mutant, together with HA-E2F1 (Fig. 6F and Western blot in fig. S5D). Together, our data support a new model by which SETD6 methylation of BRD4 at K99 plays a role in the recruitment of E2F1 to mRNA translation–related target genes for the regulation of their transcription (Fig. 6G).

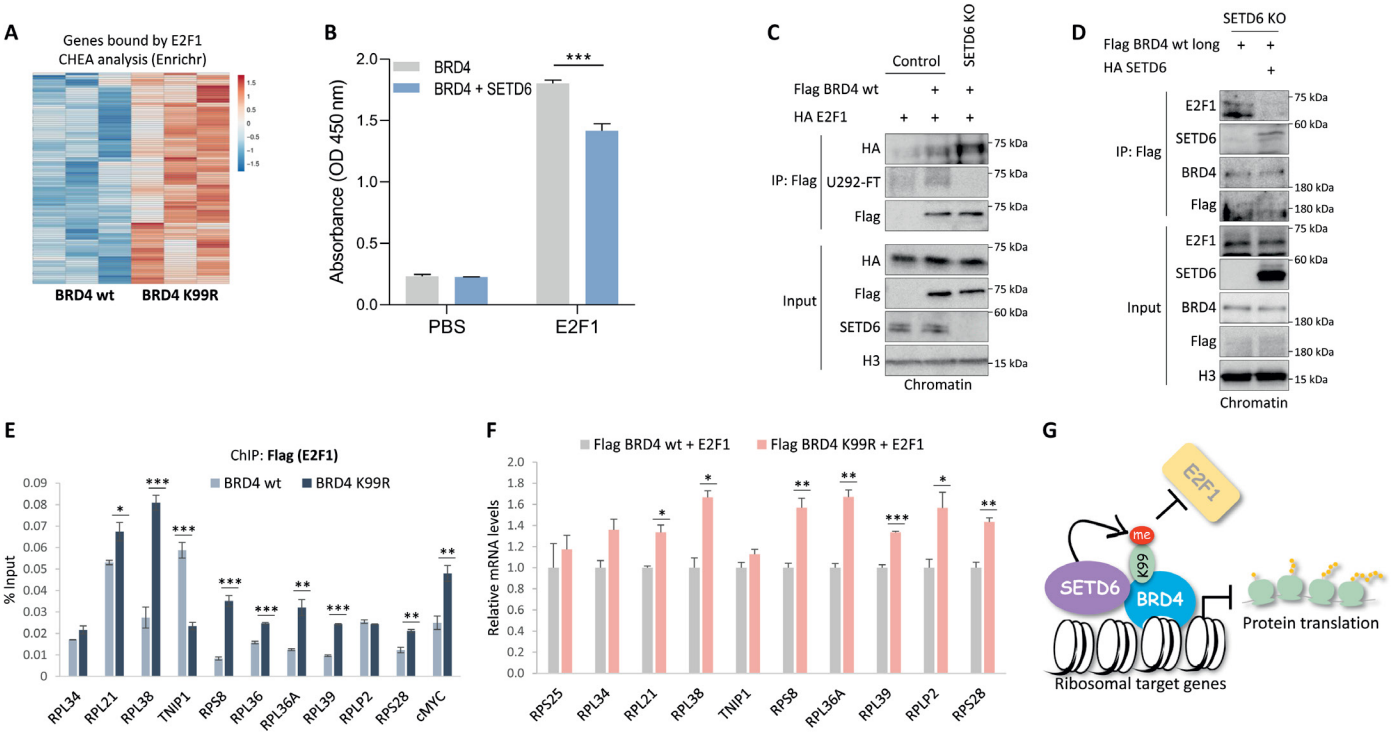

Fig. 6. BRD4 methylation at K99 controls selective binding to E2F1 to regulate transcription of genes involved in mRNA translation. (**A**) Heatmap representing 100 enriched genes for E2F1 transcription factor, analyzed by ChEA. Orange and blue colors represent higher and lower expression, respectively. (**B**) ELISA was performed with the indicated recombinant proteins preincubated in an in vitro methylation assay. Graph represents absorbance compared to phosphate-buffered saline (PBS) signal. Error bars are SD. Statistical analysis was performed for three experimental repeats using Student's *t* test. ***$P < 0.001$. OD, optical density. (**C** and **D**) MDA-MB-231 cells overexpressing the indicated plasmids were subjected to chromatin isolation and immunoprecipitation with FLAG-M2 antibody. (**E**) ChIP assay for MDA-MB-231 overexpressing Flag E2F1, with HA BRD4 wild type or HA BRD4 K99R (1-477aa). Graphs show percent input of the quantified DNA. Error bars are SEM. Statistical analysis was performed for three experimental repeats using Student's *t* test. *$P < 0.05$, **$P < 0.01$, and ***$P < 0.001$. (**F**) mRNA was extracted from MDA-MB-231 cells and transcript levels were determined by qPCR. Error bars are SEM. Statistical analysis was performed for three experimental repeats using Student's *t* test. *$P < 0.05$, **$P < 0.01$, and ***$P < 0.001$. (**G**) Schematic model illustrating the decrease of E2F1 recruitment to the chromatin and down-regulation of translation-related target gene transcription following BRD4 methylation at K99 by SETD6.

DISCUSSION

The epigenetic reader BRD4 is essential for coordinating gene expression by binding to acetylated proteins at chromatin to recruit specific factors to regulate transcription (*2*, *39*–*41*). BRD4 has been used as a therapeutic target for various inhibitors that displace it from the chromatin (*4*, *8*–*16*). However, BRD4 upstream regulation by posttranslational modifications is poorly understood. Here, we identify BRD4 as a novel substrate for methylation by SETD6. Our model suggests that methylated BRD4 at K99 inhibits the selective recruitment of the transcription factor E2F1 to translation-related target genes, leading to global translation repression (Fig. 6G).

A role for BRD4 in translation has been described before. It was shown that BRD4 down-regulation decreases the synthesis of pre-rRNA (*42*). This study found that BRD2 and BRD4 directly bind rDNA (ribosomal DNA) promoters (*42*). BRD2 and BRD4 presence at rDNA promoters is mediated by LYAR (cell growth–regulating nucleolar protein) and UBF (upstream binding factor). Together with the histone acetyltransferase KAT7, BRD2 and BRD4 promote the acetylation of histones H3 and H4 at rDNA sites to enhance rDNA transcription. Our RNA-seq experiments revealed changes in the expression of target genes that are involved in translation and splicing (Fig. 3C). However, we cannot rule out the possibility that these changes result from a compensatory effect caused by reduced activity of BRD4 following its methylation. In future experiments, using the specific K99-methyl antibody developed in our study, it would be interesting to test what the methylation status of BRD4 is in these processes and to determine whether BRD4 methylation represents another layer of regulation to fine-tune the activation/repression of genes involved in mRNA translation via recruitment of different accessory transcription factors.

E2F1, a cell proliferation and cell cycle regulator, has been reported to induce ribosome biogenesis (*36*). While BRD4 methylation does not affect ribosome association, our data suggest that SETD6 functions as a molecular switch that determines the methylation state of BRD4, which will consequently affect E2F1 recruitment to genes that are involved in mRNA translation. While the study presented here is restricted to two cell types, it would be instructive to test whether there is a tight correlation between SETD6 expression level and BRD4 methylation in other cellular systems and whether, at the genomic level, BRD4 K99 methylation correlates with the requirement for E2F1 on its target genes.

In addition to BRD4, the lysine residue K99 is conserved among the other BET family proteins, BRD2 and BRD3, but not the testis-specific BRDT (*43*). This may indicate that, similarly to BRD4, methylation of BRD2 and BRD3, which are ubiquitously expressed in various tissues (*44*, *45*), may regulate their activity. If that is the case, future experiments will allow us to determine whether it has a redundant or a specific effect. Phosphosite database interrogation (*46*) indicates that K99 in BRD4 and the corresponding lysine (K75) in BRD3 may also be subject to ubiquitination. While this observation is based only on proteomic discovery mass spectrometry experiments and was not validated biochemically by conventional methods, it still raises a very intriguing model of a competition between two different modifications.

Enhanced mRNA translation may lead to increased proliferation and transformation. Dysregulation of transcription of genes involved in mRNA translation may lead to genomic instability and cancer (*36*, *47*). Our findings suggest that selective transcription activation is mediated by a methylation signaling initiated by SETD6, which, in turn, regulates the recruitment of E2F1 to chromatin, based on the methylation status of BRD4. This molecular multistep mode of action may therefore represent a new direction for the development of new therapeutic applications.

MATERIALS AND METHODS

Plasmids

Truncated BRD4 1-477aa and BRD4 long isoform were amplified using primers indicated in Table 1. For bacterial expression, BRD4 1-477aa was cloned into pET-Duet and pET-Sumo plasmids. To generate BRD4 K99R mutation, site-directed mutagenesis on the BRD4 1-477aa vector was performed using primers indicated in Table 1. Mutated BRD4 K99R fragment was subcloned into BRD4 long isoform using Kpn I restriction enzyme. Both mutants were sequenced for confirmation. BRD4 K99R 1-477aa mutant was cloned into pET-Sumo plasmid. BRD4 1-477aa wild type and K99R mutant were cloned into pcDNA3.1 3×Flag, pcDNA3.1 3×HA, and pWZL-Flag plasmids. BRD4 long isoform wild type or K99R mutant was also cloned into pcDNA3.1 3×Flag plasmid.

SETD6 sequence was amplified by PCR and subcloned into pcDNA3.1 3×Flag and pcDNA3.1 3×HA plasmids, as previously described (*25*). For recombinant protein purification, SETD6 was cloned into pET-Duet plasmid. pET-Duet SETD6 Y285A plasmid was generated as described previously by Weil *et al.* (*30*). E2F1 sequence was amplified using primers indicated in Table 1. E2F1 was cloned into pET-Duet, pcDNA3.1 3×Flag, and pcDNA3.1 3×HA plasmids.

Cell lines, transfection, infection, and treatment

HEK293T and human breast adenocarcinoma cells (MDA-MB-231) were maintained in Dulbecco's modified Eagle's medium (Sigma-Aldrich, D5671) with 10% fetal bovine serum (Gibco), penicillin-streptomycin (Sigma-Aldrich, P0781), L-glutamine (2 mg/ml; Sigma-Aldrich, G7513), and nonessential amino acids (Sigma-Aldrich, M7145), at 37°C in a humidified incubator with 5% CO_2 as previously described (*49*). Cell transfection was performed using Mirus reagents (*Trans*IT-LT1 or *Trans*IT-X2), according to the manufacturer's instructions. CRISPR-Cas9 SETD6 KO or KD cells were generated as previously described (*25*).

Table 1. Primers for cloning and mutagenesis. FW, forward; Rev, reverse.

Name	Sequence (5′ to 3′)
BRD4 FW	TTAGGCGCGCCTCTGCGGAGAGCGGCCC
BRD4 1-477 Rev	GCCTTAATTAATCAGGTGGGAGGGGGCAC
BRD4 long Rev	GCCTTAATTAATCAGAAAAGATTTTCTTCAAATATTGACAATAG
BRD4 K99R FW	GAACCTCCCTGATTACTATAGGATCATTAAAACGCCTATGGATATG
BRD4 K99R Rev	CCATAGGCGTTTTAATGATCCTATAGTAATCAGGGAGGTTCAGC
E2F1 FW	TTAGGCGCGCCGCCTTGGCCGGGGCCCC
E2F1 Rev	GGCTTAATTAATCAGAAATCCAGGGGGGTGAGG

For stable transfection in MDA-MB-231 cell line, retroviruses were produced by transfecting HEK293T cells with the indicated pWZL constructs (empty, Flag BRD4 1-477aa wild type, or Flag BRD4 K99R) and with plasmids encoding VSV and gag-pol. Target cells were infected with the viral supernatants and selected with hygromycin B (650 μg/ml; TOKU-E). For TSA treatment, cells were treated for 4 hours with 1 μM compound or with dimethyl sulfoxide as control. TSA was provided by D. Toiber (Ben-Gurion University, Israel). For siRNA treatment, MDA-MB-231 cells were transfected with 50 nM ON-TARGETplus siControl or siBRD4 (Dharmacon, D-001810-10-05 and L-004937-00-0005, respectively) for 48 hours.

Recombinant proteins and peptides

Escherichia coli Rosetta transformed with a plasmid expressing His-tagged or His-Sumo–tagged BRD4 1-477aa wild type, BRD4 K99R mutant, E2F1, SETD6 wild type, or SETD6 Y285A mutant was grown in LB medium. Bacteria were harvested by centrifugation after isopropyl-β-D-thiogalactopyranoside induction and lysed by sonication on ice (25% amplitude, 1 min total, 10/5-s ON/OFF). His-tagged proteins were purified using Ni–nitrilotriacetic acid beads (Pierce) or on a HisTrap column (GE Healthcare) with the ÄKTA gel filtration system. Proteins were eluted by 0.5 M imidazole followed by dialysis to 10% glycerol in phosphate-buffered saline (PBS) as previously described (*48*). Recombinant GST SETD6 was expressed and purified as previously described (*22*). Purified domains His BD1, His BD2, and BRD4 were discussed before (*49*). BRD4 biotin-labeled peptide sequences were as follows: 1-unmod, N′-CDAVKLNLPDYY-KIIKTPM-C′; 1-K99me1, N′-CDAVKLNLPDYYK_{me1}IIKTPM-C′; 2-unmod, N′-LPDYYKIIKTPMDMGTIKKRLEC-C′; 2-K99me1, N′-LPDYYK_{me1}IIKTPMDMGTIKKRLEC-C′.

Antibodies, Western blot analysis, and immunoprecipitation

Primary antibodies used were as follows: anti-Flag (Sigma-Aldrich, F1804), anti-HA (Millipore, 05-904), anti-actin (Abcam, ab3280), anti-GST (Abcam, ab9085), anti-SETD6 (GeneTex, GTX629891), anti-BRD4 (Bethyl Laboratories, A700-004), puromycin (DSHB, PMY-2A4), p-6S (Cell Signaling Technology, 2215), anti-E2F1 (Cell Signaling Technology, 3742), anti–tetra-acetylated H4 (Abcam, ab177790), and anti-histone3 (H3) (Abcam, ab10799). H4 (Abcam, ab10158) was provided by A. Aharoni from Ben-Gurion University, Israel. Horseradish peroxidase (HRP)–conjugated secondary antibodies, goat anti-rabbit, goat anti-mouse, and streptavidin-HRP were obtained from Jackson ImmunoResearch (111-035-144, 115-035-062, and 016-030-084, respectively) as previously described (*48*). Anti–pan-methyl (methylated lysine antibody, HRP) was purchased from ImmuneChem (ICP0502).

For Western blot analysis, cells were homogenized and lysed in radioimmunoprecipitation assay (RIPA) buffer [50 mM tris-HCl (pH 8), 150 mM NaCl, 1% Nonidet P-40, 0.5% sodium deoxycholate, 0.1% SDS, 1 mM dithiothreitol (DTT), and 1:100 protease inhibitor mixture (Sigma-Aldrich)]. Samples were resolved on SDS–polyacrylamide gel electrophoresis (PAGE), followed by Western blot analysis. For immunoprecipitation, proteins extracted from cells were incubated for 2 hours at room temperature with FLAG-M2 magnetic beads (Sigma-Aldrich, M8823) or overnight at 4°C with FLAG-M2 beads (Sigma-Aldrich, A2220) or preconjugated A/G agarose beads (Santa Cruz Biotechnology, SC-2003) with antibody of interest. The beads were then washed three times with RIPA buffer and submitted to SDS-PAGE and Western blot analysis.

Polyclonal antibody generation

The following peptides were used to immunize two rabbits, where both animals received both peptides: CDAVKLNLPDYYK_{me1}IIKTPM (peptide 1) and LPDYYK_{me1}IIKTPMDMGTIKKRLEC (peptide 2) (Abcam, EMEA). All animal studies were ethically reviewed and carried out in accordance with Animals (Scientific Procedures) Act 1986 and the GSK Policy on the Care, Welfare, and Treatment of Animals. Antibody U292 resulted from affinity purification on peptide 1, and U293 was purified on peptide 2. On the basis of initial results, the U292 and U293 antibodies were further optimized to improve their selectivity for methylated over unmethylated BRD4 at K99 by further affinity purification of the flow-through fractions. The flow-through from U292 was purified on peptide 2 and the flow-through from U293 was purified on peptide 1. The refined antibodies are referred to as U292-FT and U293-FT.

In vitro methylation assay

Methylation assay reactions contained 4 μg of His or His-Sumo BRD4 1-477aa wild type, BRD4 K99R mutant, 1 μg of His BD1 or BD2, and 4 μg of His SETD6 or GST SETD6, 2 mCi of ^{3}H-labeled SAM (Perkin-Elmer, AdoMet), and PKMT buffer [20 mM tris-HCl (pH 8), 10% glycerol, 20 mM KCl, and 5 mM $MgCl_2$]. The reaction tubes were incubated overnight at 30°C. The reactions were resolved by SDS-PAGE for Coomassie staining (Expedeon, InstantBlue) or autoradiography. For the nonradioactive (cold) methylation assay, the ^{3}H-labeled SAM was switched to 300 μM cold SAM (Abcam, ab142221).

Semi–in vitro methylation assay

Cells were transfected with Flag BRD4 wild type or K99R plasmids. Chromatin fractions [extracted according to the protein-protein ChIP (ppChIP) protocol, see below] or cell lysates were immunoprecipitated with FLAG-M2 beads overnight at 4°C. The samples were then washed three times with RIPA buffer and once with PKMT buffer, followed by an in vitro radioactive or cold methylation assay overnight at 30°C, with or without 4 μg of His SETD6. The reactions were resolved by SDS-PAGE for Western blot analysis, Coomassie staining, or autoradiography.

Mass spectrometry

Samples of nonradioactive methylation assay containing 3 μg of His BRD4 and 4 μg of GST SETD6 were incubated with 3.2 mM SAM for different periods of time (0.5, 1, 2, 6, and 24 hours) at 30°C. An additional sample without SAM served as reference. The experiment was performed in duplicate. Samples were then digested with trypsin and submitted for liquid chromatography–tandem mass spectrometry analysis. Mass spectrometry analysis was performed with a Thermo Fisher Scientific Q-Exactive mass spectrometer (Thermo Fisher Scientific) coupled online to a nano-flow high-performance liquid chromatography system. Only in the 24-hour samples was an increased ratio of methylated/nonmethylated peptide (LNLPDYYK) identified. Mascot 2.5 (Matrix Science, Boston, MA) was used for protein identification; in a first search, 30 parts per million peptide precursor mass and 30 mDa HCD (higher-energy collisional dissociation) mass tolerance for fragment ions were used for recalibration followed by a database search using a 10 parts per million mass tolerance for peptide precursors and 20 mDa (HCD) mass tolerance for fragment ions. The search database consisted of a customized version of the SwissProt sequence database combined with a decoy version of this database created using scripts

supplied by Matrix Science, and lysine mono-methylation was used as a variable modification. Extracted ion chromatograms were generated with the Xcalibur software.

Enzyme-linked immunosorbent assay

His BRD4 (2 μg), His BD1 (5 μg), His BD2 (5 μg), or BSA diluted in PBS were added to a 96-well plate (Greiner Microlon) and incubated for 1 hour at room temperature, followed by blocking with 3% BSA for 30 min. Then, the plate was covered with 0.5 μg of GST SETD6 or GST protein (negative control) for 1 hour at room temperature. Plates were then washed and incubated with primary antibody (anti-GST, 1:4000 dilution), followed by incubation with HRP-conjugated secondary antibody (goat anti-rabbit, 1:2000 dilution) for 1 hour. Last, trimethylboron reagent and then 1 N H_2SO_4 were added; the absorbance at 450 nm was detected using a Tecan Infinite M200 plate reader. In BRD4-E2F1, ELISA conditions were as follows: His-Sumo BRD4 and His SETD6 wild type or Y285A mutant were incubated with 60 μM cold SAM at 30°C for 5 hours. The plate was covered with the reactions for 1 hour at room temperature, followed by blocking with 3% BSA overnight at 4°C. Then, the plate was covered with 1 μg of His E2F1 or 1% BSA in PBS for 2 hours. The plate was probed with anti-E2F1 primary antibody (1:1000). Signal detection was done as described above.

RNA extraction and real-time qPCR

Total RNA was extracted using the NucleoSpin RNA Kit (Macherey-Nagel). Two hundred nanograms of the extracted RNA was reverse-transcribed to complementary DNA (cDNA) using the iScript cDNA Synthesis Kit (Bio-Rad) according to the manufacturer's instructions. Real-time qPCR was performed using the UPL probe library system (Roche) in a LightCycler 480 System (Roche) as previously described (*48*). The real-time qPCR primers were designed using the universal probe library assay design center (Roche) and University of California, Santa Cruz Genome Bioinformatics (Table 2). All samples were amplified in triplicate in a 384-well plate using the following cycling conditions: 10 min at 95°C, 45 cycles of 10 s at 95°C, 30 s at 60°C, and 1 s at 72°C, followed by 30 s at 40°C. Glyceraldehyde-3-phosphate dehydrogenase (GAPDH) expression and the experiment controls were used for gene expression normalization.

Table 2. Primers for qPCR.

Name	Sequence (5′ to 3′)
GAPDH FW	AGCCACATCGCTCAGACAC
GAPDH Rev	GCCCAATACGACCAAATCC
RPS25 FW	TTGTCCGACATCTTGACGAG
RPS25 Rev	TGTCTTTCTTGGCCGACTTT
RPL34 FW	TGAGTAATAAAAATGAAAAGACGCTGT
RPL34 Rev	TGGCTCTCTCAAGCTGAGGT
RPL21 FW	GGTACCTGGGTTCAACTAAAGC
RPL21 Rev	CATAGGGAATAGGTTCCAGCA
RPL38 FW	GACGAAAGGATGCCAAATCT
RPL38 Rev	GTCAGTGATGACCAGGGTGTAA
TNIP1 FW	CAAAGATGAGGAGAAGGCAAG
TNIP1 Rev	CCACATGGTAACGCTCTCCT
RPS8 FW	AGGTTGGACGTGGGGAAT
RPS8 Rev	TCGATGATCCTTGTTTTACGAG
RPL36A FW	TGTGAGTAGACACATTTCAGGCTAA
RPL36A Rev	CACTTAACTCTTAGCAAAGACATCTCA
RPL36 FW	GGAGGAGCTGAGCAACGTA
RPL36 Rev	GGGAGGGGCTCAGTCTTT
RPS28 FW	GGTCTTGGATGTCGGGTTC
RPS28 Rev	AGGAGCATCTCAGTTACGTGTG
RPLP2 FW	ACCGGCTCAACAAGGTTATC
RPLP2 Rev	GCAGCAGAGACGGCTACAG
RPL29 FW	AGGCTCCCAAACGTACCC
RPL29 Rev	CCCATGCAGATGGTAGCC
RPL32 FW	GAAGTTCCTGGTCCACAACG
RPL32 Rev	GAGCGATCTCGGCACAGTA
RPL39 FW	CAGCTTCCCTCCTCTTCCTT
RPL39 Rev	TGGGACGATTTTGCTTTTGT
RPL8 FW	AGAAGACCCGTGTGAAGCTG
RPL8 Rev	CAAGATGGGTTTGTCAATTCG

Chromatin extraction

Chromatin fraction was isolated using ppChIP protocol, modified from a published protocol (*29*). Briefly, cells were cross-linked using 1% formaldehyde (Sigma-Aldrich) added directly to the medium and incubated on a shaking platform for 10 min at room temperature. The cross-linked reaction was stopped by adding 0.125 M glycine for 5 min. Cells were harvested and washed twice with PBS and then lysed in 1 ml of cell lysis buffer [20 mM tris-HCl (pH 8), 85 mM KCl, 0.5% Nonidet P-40, and 1:100 protease inhibitor cocktail] for 10 min on ice. Nuclear pellets were resuspended in 200 μl of nuclei lysis buffer [50 mM tris-HCl (pH 8), 10 mM EDTA, 1% SDS, and 1:100 protease inhibitor cocktail] for 10 min on ice and then sonicated (Bioruptor, Diagenode) at high-power settings for three cycles, 6 min each (30-s ON/OFF). Samples were centrifuged (13,000 rpm, 15 min, 4°C) and the soluble chromatin fraction was collected. For biochemical extraction of the chromatin, cells were harvested and resuspended in buffer A [10 mM Hepes (pH 7.9), 10 mM KCl, 1.5 mM $MgCl_2$, 0.34 M sucrose, and 10% glycerol] supplemented with 0.1% Triton X-100, 1 mM DTT, 1:200 protease inhibitor (PI) mixture, and 100 nM phenylmethylsulfonyl fluoride (PMSF; Sigma-Aldrich). Cells were incubated for 8 min on ice and then centrifuged for 5 min at 1850*g* at 4°C. The pellet was washed once with buffer A supplemented with DTT, PI, and PMSF, and then lysed with buffer B (3 mM EDTA and 0.2 mM EGTA) supplemented with DTT and PI for 30 min on ice. Samples were centrifuged for 5 min at 1850*g* at 4°C to pellet the chromatin fraction. Last, chromatin fraction was solubilized in buffer A with 1:200 benzonase nuclease enzyme (Sigma-Aldrich) and incubated for 15 min at a 37°C shaker. For immunoprecipitation, the soluble chromatin was incubated for 2 hours at room temperature with FLAG-M2 magnetic beads or overnight at 4°C with FLAG-M2 beads or precleared and incubated with Magna ChIP Protein A + G magnetic beads (Millipore, 16-663) with antibody of interest. Samples were washed according to the ppChIP protocol and analyzed by Western blot.

Chromatin preparation and ChIP-qPCR

For chromatin preparation by sonication, cells were prepared as described in the ppChIP protocol, except for the sonication settings, which were set to six cycles, 6 min each cycle (30-s ON/OFF). Chromatin immunoprecipitation was performed as previously described (*50*, *51*). The chromatin fraction was diluted 5× in dilution buffer [20 mM tris-HCl (pH 8), 2 mM EDTA, 150 mM NaCl, 1.84% Triton X-100, and 0.2% SDS]. Chromatin was precleared overnight at 4°C with nProtein A Sepharose 4 Fast Flow Beads (GE Healthcare, 17-5280-01). The precleared sample was then immunoprecipitated in dilution buffer with FLAG-M2 beads or nProtein A Sepharose beads preconjugated with polyclonal rabbit BRD4 K99me1 antibody. The immunoprecipitated complexes were washed once with TSE150 buffer [20 mM tris-HCl (pH 8), 2 mM EDTA, 1% Triton X-100, 0.1% SDS, and 150 mM NaCl], TSE500 buffer [20 mM tris-HCl (pH 8), 2 mM EDTA, 1% Triton X-100, 0.1% SDS, and 500 mM NaCl], buffer 3 [250 mM LiCl, 10 mM tris-HCl (pH 8), 1 mM EDTA, 1% sodium deoxycholate, and 1% Nonidet P-40], and twice with TE buffer [10 mM tris-HCl (pH 8) and 1 mM EDTA]. DNA was eluted with elution buffer (50 mM $NaHCO_3$, 140 mM NaCl, and 1% SDS) containing ribonuclease A (0.2 μg/μl) and proteinase K (0.2 μg/μl). Last, the DNA eluates were decross-linked at 65°C overnight with shaking at 900 rpm and purified by NucleoSpin Gel and PCR Clean-up kit (Macherey-Nagel), according to the manufacturer's instructions. Purified DNA was subjected to qPCR using specific primers (Table 3). Primers were designed on the basis of BRD4 occupancy found in different ChIP-seq data previously published in National Center for Biotechnology Information Gene Expression Omnibus (GEO) datasets by Xiong *et al.* (*52*) (GEO accession: GSE123097), Rhie *et al.* (*53*) (GEO accession: GSE49651), Messier *et al.* (*54*) (GEO accession: GSE69377), and Zanconato *et al.* (*55*) (GEO accession: GSE102406) and viewed using Integrated Genomics Viewer software (*56*). qPCR was preformed using SYBR Green I Master (Roche) in a LightCycler 480 System (Roche). All samples were amplified in triplicate in a 384-well plate using the following cycling conditions: 5 min at 95°C, 45 cycles of amplification; 10 s at 95°C, 10 s at 60°C, and 10 s at 72°C, followed by melting curve acquisition; and 5 s at 95°C, 1 min at 65°C and monitoring up to 97°C, and lastly cooling for 30 s at 40°C. The results were normalized to input DNA and presented as % input.

Table 3. Primers for ChIP-qPCR.

Name	Sequence (5′ to 3′)
cMYC ChIP FW	AATTCCAGCGAGAGGCAGAG
cMYC ChIP Rev	GAAGCCCCCTATTCGCTCC
TNIP1 ChIP FW	GAGGCTCTGGACGATCTGGG
TNIP1 ChIP Rev	CTCCCCGTCCTCGGGTAAG
RPL34 ChIP FW	GTCCTTTGAGCTGGTGTAGGG
RPL34 ChIP Rev	GCTGTGGCTACTCACGGCT
RPL21 ChIP FW	GGCCTCAGAGGTCGTTCATT
RPL21 ChIP Rev	ACATGGTTTAACCCGCCCAT
RPL38 ChIP FW	CGATATTTCGGGGGAGAGCG
RPL38 ChIP Rev	GACCTGCGGGAAACAGTCC
RPS8 ChIP FW	AGCCTACTGAGGAGTCCAGA
RPS8 ChIP Rev	CGAAACCCGAGGGCCAC
RPL36A ChIP FW	GGCCGAGTAACATCCAGCTT
RPL36A ChIP Rev	GTTGATCCCGGCAAGATTGG
RPL36 ChIP FW	AGGTTGGAGGATGGTTGGTT
RPL36 ChIP Rev	GAGAAGGGGCGGAGGTGA
RPS28 ChIP FW	GGAGGGATTAGAGGAGCCAA
RPS28 ChIP Rev	CGTGCACTGTCCCTGAGAA
RPLP2 ChIP FW	CCTTTGGACTCGCTTCGTC
RPLP2 ChIP Rev	GTTCCGGAAGTGACTGCTCT

RNA-seq and data processing

Total RNA was extracted from MDA-MB-231 cells with different treatments, using the NucleoSpin RNA Kit (Macherey-Nagel), according to the manufacturer's instructions. Samples were prepared in triplicate. Barcoded stranded mRNA-seq libraries were prepared at European Molecular Biology Laboratory Genomic Core Facilities (Heidelberg, Germany) from high-quality total RNA samples (~500 ng per sample) using the Illumina TruSeq RNA Sample Preparation v2 Kit in the workflow implemented on the liquid-handling robot Beckman FXP2. Obtained libraries that passed the QC (quality control) step were combined in equimolar amounts into pools of eight libraries; 10 pM solution of each pool was loaded per lane of the Illumina sequencer HiSeq 2500 flow cell and sequenced unidirectionally with the Illumina v4 chemistry, generating ~220 million reads per lane, each 50 bases long, and then aligned to the human genome reference hg38 and quantified.

Bioinformatic analysis

Bioinformatic analysis of the RNA-seq data was carried out using NeatSeq-Flow (*57*) and R. Raw sequence reads underwent quality assessment with FASTQC and MultiQC, followed by quality trimming with Trim Galore!. Clean reads were aligned to the human genome version GRCh38 (Ensembl) using STAR, and gene expression was estimated with RSEM (RNA-Seq by Expectation-Maximization). Subsequent analysis was done for each experiment (CRISPR SETD6 and stable BRD4 cells) separately. For quality assessment, counts underwent variance-stabilizing transformation [DESeq2 (*58*)] and submitted to sample-wise correlation analysis and principal components analysis. Statistical testing for differential expression was carried out using DESeq2, a method specifically tailored for count data by use of negative binomial generalized linear models.

For hierarchical clustering, genes were selected according to the following criteria: in the SETD6 experiment, annotated genes (i.e., having a gene symbol) that were either up-regulated or down-regulated [false discovery rate (FDR)–adjusted P value < 0.05] in all KO/KD treatments versus the control; in the BRD4 experiment, annotated genes in the up-regulated or down-regulated category (FDR-adjusted P value < 0.05) in BRD4 K99R versus BRD4 wild type comparison, and significantly changed (either up- or down-regulated) in BRD4 wild-type versus empty comparison. Hierarchical clustering, after z-scoring of their variance-stabilized expression values, was carried out using the ClustVis web tool (https://biit.cs.ut.ee/clustvis/) (*59*). Enrichment for gene ontology biological processes and KEGG pathways was performed using DAVID (https://david.ncifcrf.gov/) (*60*, *61*).

ChEA was performed using Enrichr database (*62*, *63*). The 275 up-regulated genes identified in RNA-seq of BRD4 K99R compared to BRD4 wild-type cells were submitted to ChEA gene analysis. The

identified genes were visualized in a heatmap, created using the ClustVis web tool (https://biit.cs.ut.ee/clustvis/) (*59*).

Translation assay

For the translation assay performed using the SUnSET method (*31*), cells were treated with puromycin (10 μg/ml) for 10 min. Cells were then lysed in RIPA buffer and submitted to Western blot to detect protein synthesis using anti-puromycin antibody.

Polysome profiling

Polysome profiling was performed as previously published by Liang *et al.* (*64*). Briefly, cells were treated with cycloheximide (100 μg/ml) for 10 min, then washed with PBS that contained cycloheximide (100 μg/ml), and collected by centrifugation at 300*g* for 5 min at 4°C. Cells were lysed in a hypotonic lysis buffer (50 mM tris-base, 2.5 mM $MgCl_2$, 1.5 mM KCl, 5.5% Triton X-100, 0.5% sodium deoxycholate, and 2 mM DTT) containing cycloheximide (100 μg/ml) and RNaseOUT (0.24 U/μl; Thermo Fisher Scientific, 10777019), vortexed, and centrifuged at 17,800*g* for 2 min at 4°C. Fifty microliters of the samples was saved (total cell lysate), and the rest were loaded on the top of a three-layer sucrose gradient tube followed by ultracentrifugation at 36,000 rpm for 2.5 hours at 4°C. Monosome and polysome fractions were collected using a piston gradient collector (Biocomp) fitted with an ultraviolet detector (Tirax). Samples were then dialyzed in PBS buffer and concentrated using Amicon Ultra 0.5-ml Centrifugal Filters (Merck). All samples were resolved on SDS-PAGE and subjected to Western blot analysis.

Statistical analyses

Statistical analyses for all assays were performed with GraphPad Prism software, using Student's two-tailed *t* test (unpaired) and one-way or two-way analysis of variance (ANOVA) with a Tukey's post hoc test.

SUPPLEMENTARY MATERIALS

Supplementary material for this article is available at http://advances.sciencemag.org/cgi/content/full/7/22/eabf5374/DC1

View/request a protocol for this paper from *Bio-protocol*.

REFERENCES AND NOTES

1. J. L. Morgado-Pascual, S. Rayego-Mateos, L. Tejedor, B. Suarez-Alvarez, M. Ruiz-Ortega, Bromodomain and extraterminal proteins as novel epigenetic targets for renal diseases. *Front. Pharmacol.* **10**, 1315 (2019).
2. P. Filippakopoulos, S. Knapp, Targeting bromodomains: Epigenetic readers of lysine acetylation. *Nat. Rev. Drug Discov.* **13**, 337–356 (2014).
3. A. Hajmirza, A. Emadali, A. Gauthier, O. Casasnovas, R. Gressin, M. B. Callanan, BET family protein BRD4: An emerging actor in NFκB signaling in inflammation and cancer. *Biomedicine* **6**, 16 (2018).
4. J. Shi, Y. Wang, L. Zeng, Y. Wu, J. Deng, Q. Zhang, Y. Lin, J. Li, T. Kang, M. Tao, E. Rusinova, G. Zhang, C. Wang, H. Zhu, J. Yao, Y.-X. Zeng, B. M. Evers, M.-M. Zhou, B. P. Zhou, Disrupting the interaction of BRD4 with diacetylated Twist suppresses tumorigenesis in basal-like breast cancer. *Cancer Cell* **25**, 210–225 (2014).
5. Z. Yang, N. He, Q. Zhou, Brd4 recruits P-TEFb to chromosomes at late mitosis to promote G_1 gene expression and cell cycle progression. *Mol. Cell. Biol.* **28**, 967–976 (2008).
6. Z. Yang, J. H. N. Yik, R. Chen, N. He, M. K. Jang, K. Ozato, Q. Zhou, Recruitment of P-TEFb for stimulation of transcriptional elongation by the bromodomain protein Brd4. *Mol. Cell* **19**, 535–545 (2005).
7. M. K. Jang, K. Mochizuki, M. Zhou, H.-S. Jeong, J. N. Brady, K. Ozato, The bromodomain protein Brd4 is a positive regulatory component of P-TEFb and stimulates RNA polymerase II-dependent transcription. *Mol. Cell* **19**, 523–534 (2005).
8. M. A. Dawson, E. J. Gudgin, S. J. Horton, G. Giotopoulos, E. Meduri, S. Robson, E. Cannizzaro, H. Osaki, M. Wiese, S. Putwain, C. Y. Fong, C. Grove, J. Craig, A. Dittmann, D. Lugo, P. Jeffrey, G. Drewes, K. Lee, L. Bullinger, R. K. Prinjha, T. Kouzarides, G. S. Vassiliou, B. J. P. Huntly, Recurrent mutations, including NPM1c, activate a BRD4-dependent core transcriptional program in acute myeloid leukemia. *Leukemia* **28**, 311–320 (2014).
9. O. Gilan, I. Rioja, K. Knezevic, M. J. Bell, M. M. Yeung, N. R. Harker, E. Y. N. Lam, C.-w. Chung, P. Bamborough, M. Petretich, M. Urh, S. J. Atkinson, A. K. Bassil, E. J. Roberts, D. Vassiliadis, M. L. Burr, A. G. S. Preston, C. Wellaway, T. Werner, J. R. Gray, A.-M. Michon, T. Gobbetti, V. Kumar, P. E. Soden, A. Haynes, J. Vappiani, D. F. Tough, S. Taylor, S.-J. Dawson, M. Bantscheff, M. Lindon, G. Drewes, E. H. Demont, D. L. Daniels, P. Grandi, R. K. Prinjha, M. A. Dawson, Selective targeting of BD1 and BD2 of the BET proteins in cancer and immunoinflammation. *Science* **368**, 387–394 (2020).
10. Z. Yao, S. Yang, H. Zhao, H. Yang, X. Jiang, BET inhibitor I-BET151 sensitizes GBM cells to temozolomide via PUMA induction. *Cancer Gene Ther.* **27**, 226–234 (2020).
11. A. Liu, D. Fan, Y. Wang, The BET bromodomain inhibitor i-BET151 impairs ovarian cancer metastasis and improves antitumor immunity. *Cell Tissue Res.* **374**, 577–585 (2018).
12. C. Y. Fong, O. Gilan, E. Y. N. Lam, A. F. Rubin, S. Ftouni, D. Tyler, K. Stanley, D. Sinha, P. Yeh, J. Morison, G. Giotopoulos, D. Lugo, P. Jeffrey, S. C.-W. Lee, C. Carpenter, R. Gregory, R. G. Ramsay, S. W. Lane, O. Abdel-Wahab, T. Kouzarides, R. W. Johnstone, S.-J. Dawson, B. J. P. Huntly, R. K. Prinjha, A. T. Papenfuss, M. A. Dawson, BET inhibitor resistance emerges from leukaemia stem cells. *Nature* **525**, 538–542 (2015).
13. A. Chaidos, V. Caputo, K. Gouvedenou, B. Liu, I. Marigo, M. S. Chaudhry, A. Rotolo, D. F. Tough, N. N. Smithers, A. K. Bassil, T. D. Chapman, N. R. Harker, O. Barbash, P. Tummino, N. Al-Mahdi, A. C. Haynes, L. Cutler, B. C. Le, A. Rahemtulla, I. Roberts, M. Kleijnen, J. J. Witherington, N. J. Parr, R. K. Prinjha, A. Karadimitris, Potent antimyeloma activity of the novel bromodomain inhibitors I-BET151 and I-BET762. *Blood* **123**, 697–705 (2014).
14. M. A. Dawson, R. K. Prinjha, A. Dittmann, G. Giotopoulos, M. Bantscheff, W.-I. Chan, S. C. Robson, C.-w. Chung, C. Hopf, M. M. Savitski, C. Huthmacher, E. Gudgin, D. Lugo, S. Beinke, T. D. Chapman, E. J. Roberts, P. E. Soden, K. R. Auger, O. Mirguet, K. Doehner, R. Delwel, A. K. Burnett, P. Jeffrey, G. Drewes, K. Lee, B. J. P. Huntly, T. Kouzarides, Inhibition of BET recruitment to chromatin as an effective treatment for MLL-fusion leukaemia. *Nature* **478**, 529–533 (2011).
15. J. E. Delmore, G. C. Issa, M. E. Lemieux, P. B. Rahl, J. Shi, H. M. Jacobs, E. Kastritis, T. Gilpatrick, R. M. Paranal, J. Qi, M. Chesi, A. C. Schinzel, M. R. McKeown, T. P. Heffernan, C. R. Vakoc, P. L. Bergsagel, I. M. Ghobrial, P. G. Richardson, R. A. Young, W. C. Hahn, K. C. Anderson, A. L. Kung, J. E. Bradner, C. S. Mitsiades, BET bromodomain inhibition as a therapeutic strategy to target c-Myc. *Cell* **146**, 904–917 (2011).
16. P. Filippakopoulos, J. Qi, S. Picaud, Y. Shen, W. B. Smith, O. Fedorov, E. M. Morse, T. Keates, T. T. Hickman, I. Felletar, M. Philpott, S. Munro, M. R. McKeown, Y. Wang, A. L. Christie, N. West, M. J. Cameron, B. Schwartz, T. D. Heightman, N. L. Thangue, C. A. French, O. Wiest, A. L. Kung, S. Knapp, J. E. Bradner, Selective inhibition of BET bromodomains. *Nature* **468**, 1067–1073 (2010).
17. H. Alam, B. Gu, M. G. Lee, Histone methylation modifiers in cellular signaling pathways. *Cell. Mol. Life Sci.* **72**, 4577–4592 (2015).
18. R. Hamamoto, V. Saloura, Y. Nakamura, Critical roles of non-histone protein lysine methylation in human tumorigenesis. *Nat. Rev. Cancer* **15**, 110–124 (2015).
19. E. M. Cornett, L. Ferry, P.-A. Defossez, S. B. Rothbart, Lysine methylation regulators moonlighting outside the epigenome. *Mol. Cell* **75**, 1092–1101 (2019).
20. D. Levy, Lysine methylation signaling of non-histone proteins in the nucleus. *Cell. Mol. Life Sci.* **76**, 2873–2883 (2019).
21. D. Han, M. Huang, T. Wang, Z. Li, Y. Chen, C. Liu, Z. Lei, X. Chu, Lysine methylation of transcription factors in cancer. *Cell Death Dis.* **10**, 290 (2019).
22. D. Levy, A. J. Kuo, Y. Chang, U. Schaefer, C. Kitson, P. Cheung, A. Espejo, B. M. Zee, C. L. Liu, S. Tangsombatvisit, R. I. Tennen, A. Y. Kuo, S. Tanjing, R. Cheung, K. F. Chua, P. J. Utz, X. Shi, R. K. Prinjha, K. Lee, B. A. Garcia, M. T. Bedford, A. Tarakhovsky, X. Cheng, O. Gozani, Lysine methylation of the NF-κB subunit RelA by SETD6 couples activity of the histone methyltransferase GLP at chromatin to tonic repression of NF-κB signaling. *Nat. Immunol.* **12**, 29–36 (2011).
23. M. Feldman, Z. Vershinin, I. Goliand, N. Elia, D. Levy, The methyltransferase SETD6 regulates mitotic progression through PLK1 methylation. *Proc. Natl. Acad. Sci. U.S.A.* **116**, 1235–1240 (2019).
24. R. Yao, Y. Wang, D. Han, Y. Ma, M. Ma, Y. Zhao, J. Tan, J. Lu, G. Xu, X. Li, Lysines 207 and 325 methylation of WDR5 catalyzed by SETD6 promotes breast cancer cell proliferation and migration. *Oncol. Rep.* **40**, 3069–3077 (2018).
25. Z. Vershinin, M. Feldman, A. Chen, D. Levy, PAK4 methylation by SETD6 promotes the activation of the Wnt/β-Catenin pathway. *J. Biol. Chem.* **291**, 6786–6795 (2016).
26. A. Chen, M. Feldman, Z. Vershinin, D. Levy, SETD6 is a negative regulator of oxidative stress response. *Biochim. Biophys. Acta* **1859**, 420–427 (2016).
27. D. J. O'Neill, S. C. Williamson, D. Alkharaif, I. C. Monteiro, M. Goudreault, L. Gaughan, C. N. Robson, A. C. Gingras, O. Binda, SETD6 controls the expression of estrogen-responsive genes and proliferation of breast carcinoma cells. *Epigenetics* **9**, 942–950 (2014).
28. O. Binda, A. Sevilla, G. LeRoy, I. R. Lemischka, B. A. Garcia, S. Richard, SETD6 monomethylates H2AZ on lysine 7 and is required for the maintenance of embryonic stem cell self-renewal. *Epigenetics* **8**, 177–183 (2013).

29. R. M. Ricke, A.-K. Bielinsky, Easy detection of chromatin binding proteins by the histone association assay. *Biol. Proced. Online* **7**, 60–69 (2005).
30. L. E. Weil, Y. Shmidov, M. Kublanovsky, D. Morgenstern, M. Feldman, R. Bitton, D. Levy, Oligomerization and auto-methylation of the human lysine methyltransferase SETD6. *J. Mol. Biol.* **430**, 4359–4368 (2018).
31. E. K. Schmidt, G. Clavarino, M. Ceppi, P. Pierre, SUnSET, a nonradioactive method to monitor protein synthesis. *Nat. Methods* **6**, 275–277 (2009).
32. L. Handoko, B. Kaczkowski, C. C. Hon, M. Lizio, M. Wakamori, T. Matsuda, T. Ito, P. Jeyamohan, Y. Sato, K. Sakamoto, S. Yokoyama, H. Kimura, A. Minoda, T. Umehara, JQ1 affects BRD2-dependent and independent transcription regulation without disrupting H4-hyperacetylated chromatin states. *Epigenetics* **13**, 410–431 (2018).
33. J.-P. Lambert, S. Picaud, T. Fujisawa, H. Hou, P. Savitsky, L. Uusküla-Reimand, G. D. Gupta, H. Abdouni, Z.-Y. Lin, M. Tucholska, J. D. R. Knight, B. Gonzalez-Badillo, N. St-Denis, J. A. Newman, M. Stucki, L. Pelletier, N. Bandeira, M. D. Wilson, P. Filippakopoulos, A.-C. Gingras, Interactome rewiring following pharmacological targeting of BET bromodomains. *Mol. Cell* **73**, 621–638.e17 (2019).
34. P. Filippakopoulos, S. Picaud, M. Mangos, T. Keates, J.-P. Lambert, D. Barsyte-Lovejoy, I. Felletar, R. Volkmer, S. Müller, T. Pawson, A.-C. Gingras, C. H. Arrowsmith, S. Knapp, Histone recognition and large-scale structural analysis of the human bromodomain family. *Cell* **149**, 214–231 (2012).
35. A. Lachmann, H. Xu, J. Krishnan, S. I. Berger, A. R. Mazloom, A. Ma'ayan, ChEA: Transcription factor regulation inferred from integrating genome-wide ChIP-X experiments. *Bioinformatics* **26**, 2438–2444 (2010).
36. S. Vadivel Gnanasundram, R. Fåhraeus, Translation stress regulates ribosome synthesis and cell proliferation. *Int. J. Mol. Sci.* **19**, 3757 (2018).
37. S. Real, N. Meo-Evoli, L. Espada, A. Tauler, E2F1 regulates cellular growth by mTORC1 signaling. *PLOS ONE* **6**, e16163 (2011).
38. O. Ayrault, L. Andrique, P. Séité, Involvement of the transcriptional factor E2F1 in the regulation of the rRNA promoter. *Exp. Cell Res.* **312**, 1185–1193 (2006).
39. A. Zippo, R. Serafini, M. Rocchigiani, S. Pennacchini, A. Krepelova, S. Oliviero, Histone crosstalk between H3S10ph and H4K16ac generates a histone code that mediates transcription elongation. *Cell* **138**, 1122–1136 (2009).
40. E. P. Blankenhorn, Comparative immunogenetics of the major histocompatibility complex. *Immunol. Ser.* **43**, 287–318 (1989).
41. H. J. Trappe, C. A. Hartwig, H. Klein, P. Wenzlaff, P. R. Lichtlen, Incidence of sudden cardiac death in patients with 2-vessel coronary disease in relation to anatomy and rhythm profile. *Z. Kardiol.* **77**, 1–8 (1988).
42. K. Izumikawa, H. Ishikawa, H. Yoshikawa, S. Fujiyama, A. Watanabe, H. Aburatani, H. Tachikawa, T. Hayano, Y. Miura, T. Isobe, R. J. Simpson, L. Li, J. Min, N. Takahashi, LYAR potentiates rRNA synthesis by recruiting BRD2/4 and the MYST-type acetyltransferase KAT7 to rDNA. *Nucleic Acids Res.* **47**, 10357–10372 (2019).
43. S.-Y. Wu, C.-M. Chiang, The double bromodomain-containing chromatin adaptor Brd4 and transcriptional regulation. *J. Biol. Chem.* **282**, 13141–13145 (2007).
44. A. Stathis, F. Bertoni, BET proteins as targets for anticancer treatment. *Cancer Discov.* **8**, 24–36 (2018).
45. E. Shang, G. Salazar, T. E. Crowley, X. Wang, R. A. Lopez, X. Wang, D. J. Wolgemuth, Identification of unique, differentiation stage-specific patterns of expression of the bromodomain-containing genes *Brd2, Brd3, Brd4*, and *Brdt* in the mouse testis. *Gene Expr. Patterns* **4**, 513–519 (2004).
46. P. V. Hornbeck, B. Zhang, B. Murray, J. M. Kornhauser, V. Latham, E. Skrzypek, PhosphoSitePlus, 2014: Mutations, PTMs and recalibrations. *Nucleic Acids Res.* **43**, D512–D520 (2015).
47. D. Ruggero, P. P. Pandolfi, Does the ribosome translate cancer? *Nat. Rev. Cancer* **3**, 179–192 (2003).
48. Z. Vershinin, M. Feldman, D. Levy, PAK4 methylation by the methyltransferase SETD6 attenuates cell adhesion. *Sci. Rep.* **10**, 17068 (2020).
49. C.-w. Chung, H. Coste, J. H. White, O. Mirguet, J. Wilde, R. L. Gosmini, C. Delves, S. M. Magny, R. Woodward, S. A. Hughes, E. V. Boursier, H. Flynn, A. M. Bouillot, P. Bamborough, J.-M. G. Brusq, F. J. Gellibert, E. J. Jones, A. M. Riou, P. Homes, S. L. Martin, I. J. Uings, J. Toum, C. A. Clément, A.-B. Boullay, R. L. Grimley, F. M. Blandel, R. K. Prinjha, K. Lee, J. Kirilovsky, E. Nicodeme, Discovery and characterization of small molecule inhibitors of the BET family bromodomains. *J. Med. Chem.* **54**, 3827–3838 (2011).
50. S. Mishra, C. Van Rechem, S. Pal, T. L. Clarke, D. Chakraborty, S. D. Mahan, J. C. Black, S. E. Murphy, M. S. Lawrence, D. L. Daniels, J. R. Whetstine, Cross-talk between lysine-modifying enzymes controls site-specific DNA amplifications. *Cell* **174**, 803–817.e16 (2018).
51. E. Ainbinder, M. Revach, O. Wolstein, S. Moshonov, N. Diamant, R. Dikstein, Mechanism of rapid transcriptional induction of tumor necrosis factor alpha-responsive genes by NF-κB. *Mol. Cell. Biol.* **22**, 6354–6362 (2002).
52. L. Xiong, F. Wu, Q. Wu, L. Xu, O. K. Cheung, W. Kang, M. T. Mok, L. L. M. Szeto, C.-Y. Lun, R. W. Lung, J. Zhang, K. H. Yu, S.-D. Lee, G. Huang, C.-M. Wang, J. Liu, Z. Yu, D.-Y. Yu, J.-L. Chou, W.-H. Huang, B. Feng, Y.-S. Cheung, P. B. Lai, P. Tan, N. Wong, M. W. Chan, T. H. Huang, K. Y. Yip, A. S. Cheng, K.-F. To, Aberrant enhancer hypomethylation contributes to hepatic carcinogenesis through global transcriptional reprogramming. *Nat. Commun.* **10**, 335 (2019).
53. S. K. Rhie, D. J. Hazelett, S. G. Coetzee, C. Yan, H. Noushmehr, G. A. Coetzee, Nucleosome positioning and histone modifications define relationships between regulatory elements and nearby gene expression in breast epithelial cells. *BMC Genomics* **15**, 331 (2014).
54. T. L. Messier, J. A. Gordon, J. R. Boyd, C. E. Tye, G. Browne, J. L. Stein, J. B. Lian, G. S. Stein, Histone H3 lysine 4 acetylation and methylation dynamics define breast cancer subtypes. *Oncotarget* **7**, 5094–5109 (2016).
55. F. Zanconato, G. Battilana, M. Forcato, L. Filippi, L. Azzolin, A. Manfrin, E. Quaranta, D. D. Biagio, G. Sigismondo, V. Guzzardo, P. Lejeune, B. Haendler, J. Krijgsveld, M. Fassan, S. Bicciato, M. Cordenonsi, S. Piccolo, Transcriptional addiction in cancer cells is mediated by YAP/TAZ through BRD4. *Nat. Med.* **24**, 1599–1610 (2018).
56. J. T. Robinson, H. Thorvaldsdottir, W. Winckler, M. Guttman, E. S. Lander, G. Getz, J. P. Mesirov, Integrative genomics viewer. *Nat. Biotechnol.* **29**, 24–26 (2011).
57. M. Sklarz, L. Levin, M. Gordon, V. Chalifa-Caspi, NeatSeq-Flow: A lightweight high-throughput sequencing workflow platform for non-programmers and programmers alike. *bioRxiv* , 173005 (2018).
58. M. I. Love, W. Huber, S. Anders, Moderated estimation of fold change and dispersion for RNA-seq data with DESeq2. *Genome Biol.* **15**, 550 (2014).
59. T. Metsalu, J. Vilo, ClustVis: A web tool for visualizing clustering of multivariate data using principal component analysis and heatmap. *Nucleic Acids Res.* **43**, W566–W570 (2015).
60. D. W. Huang, B. T. Sherman, R. A. Lempicki, Systematic and integrative analysis of large gene lists using DAVID bioinformatics resources. *Nat. Protoc.* **4**, 44–57 (2009).
61. D. W. Huang, B. T. Sherman, R. A. Lempicki, Bioinformatics enrichment tools: Paths toward the comprehensive functional analysis of large gene lists. *Nucleic Acids Res.* **37**, 1–13 (2009).
62. M. V. Kuleshov, M. R. Jones, A. D. Rouillard, N. F. Fernandez, Q. Duan, Z. Wang, S. Koplev, S. L. Jenkins, K. M. Jagodnik, A. Lachmann, M. G. McDermott, C. D. Monteiro, G. W. Gundersen, A. Ma'ayan, Enrichr: A comprehensive gene set enrichment analysis web server 2016 update. *Nucleic Acids Res.* **44**, W90–W97 (2016).
63. E. Y. Chen, C. M. Tan, Y. Kou, Q. Duan, Z. Wang, G. V. Meirelles, N. R. Clark, A. Ma'ayan, Enrichr: Interactive and collaborative HTML5 gene list enrichment analysis tool. *BMC Bioinformatics* **14**, 128 (2013).
64. S. Liang, H. M. Bellato, J. Lorent, F. C. S. Lupinacci, C. Oertlin, V. van Hoef, V. P. Andrade, M. Roffe, L. Masvidal, G. N. M. Hajj, O. Larsson, Polysome-profiling in small tissue samples. *Nucleic Acids Res.* **46**, e3 (2018).

Acknowledgments: This paper is dedicated to the memory of my dearest father and an inspiring scientist, Professor Yossi Levy, who passed away while this paper was being peer-reviewed. We thank the Levy lab for technical assistance and helpful discussions. We thank V. Benes and GeneCore for the RNA-seq library preparation and sequencing. **Funding:** This work was supported by grants to D.L. from the Israel Science Foundation (285/14 and 262/18), the Research Career Development Award from the Israel Cancer Research Fund, and the Israel Cancer Association. B.R. acknowledges support from the Israel Science Foundation (1436/19).
Author contributions: Z.V., M.F., and D.L. conceived and designed the majority of the experiments. T.W. and M.B. performed the mass spectrometry analysis, and T.C. and L.E.W. assisted in the experiments to validate the BRD4 K99me1 antibody. K.A. and B.R. performed the polysome profiling experiments, and L.E.W., M.K., and E.A.-S. performed some of the IP experiments. V.C.-C., M.S., E.Y.N.L., and M.A.D. performed the bioinformatic analysis. S.P., P.F., H.D.L., P.G., and M.K. helped with experimental design and provided valuable conceptual input for the study. Z.V., M.F., and D.L. wrote the paper. All authors read and approved the final manuscript. **Competing interests:** The following authors are employees and/or shareholders of GlaxoSmithKline (GSK): T.W., R.A.M., M.B., T.C., H.D.L., P.G., and R.K.P. M.A.D. has been a member of advisory boards for GlaxoSmithKline, CTX CRC, Storm Therapeutics, Celgene, and Cambridge Epigenetix. The other authors declare that they have no competing interests. **Data and materials availability:** All data needed to evaluate the conclusions in the paper are present in the paper and/or the Supplementary Materials. Additional data related to this paper may be requested from the authors.

Submitted 2 November 2020
Accepted 6 April 2021
Published 26 May 2021
10.1126/sciadv.abf5374

Citation: Z. Vershinin, M. Feldman, T. Werner, L. E. Weil, M. Kublanovsky, E. Abaev-Schneiderman, M. Sklarz, E. Y. N. Lam, K. Alasad, S. Picaud, B. Rotblat, R. A. McAdam, V. Chalifa-Caspi, M. Bantscheff, T. Chapman, H. D. Lewis, P. Filippakopoulos, M. A. Dawson, P. Grandi, R. K. Prinjha, D. Levy, BRD4 methylation by the methyltransferase SETD6 regulates selective transcription to control mRNA translation. *Sci. Adv.* **7**, eabf5374 (2021).

RESEARCH ARTICLES

CANCER

Cancer cells use self-inflicted DNA breaks to evade growth limits imposed by genotoxic stress

Brian D. Larsen[1], Jan Benada[1], Philip Yuk Kwong Yung[2]†, Ryan A. V. Bell[3]†, George Pappas[4]†, Vaclav Urban[5], Johanna K. Ahlskog[1], Tia T. Kuo[1], Pavel Janscak[5,6], Lynn A. Megeney[3], Simon J. Elsässer[2], Jiri Bartek[2,4,5], Claus S. Sørensen[1]*

Genotoxic therapy such as radiation serves as a frontline cancer treatment, yet acquired resistance that leads to tumor reoccurrence is frequent. We found that cancer cells maintain viability during irradiation by reversibly increasing genome-wide DNA breaks, thereby limiting premature mitotic progression. We identify caspase-activated DNase (CAD) as the nuclease inflicting these de novo DNA lesions at defined loci, which are in proximity to chromatin-modifying CCCTC-binding factor (CTCF) sites. CAD nuclease activity is governed through phosphorylation by DNA damage response kinases, independent of caspase activity. In turn, loss of CAD activity impairs cell fate decisions, rendering cancer cells vulnerable to radiation-induced DNA double-strand breaks. Our observations highlight a cancer-selective survival adaptation, whereby tumor cells deploy regulated DNA breaks to delimit the detrimental effects of therapy-evoked DNA damage.

Genotoxic cancer therapy inactivates and kills cancer cells by inflicting extensive DNA damage. Radiation therapy (RT) is the most broadly applied genotoxic challenge in standard-of-care oncological treatment. The deposition of energy as radiation passes through the genetic material triggers extensive DNA lesions often in the form of double-strand breaks (DSBs), single-stranded breaks (SSBs), and interstrand cross-links (*1*). The extent of this damage can present an insurmountable barrier to cellular fitness, triggering cell death or cell cycle withdrawal. Facilitating the DNA damage response (DDR) and lesion repair while avoiding cell death and cell cycle blockage is critical for cell survival after RT. Clinically, resistance to RT remains a considerable obstacle to effective tumor control, as the cancer cells deploy an arsenal of mechanisms, still incompletely understood, to mitigate the effects of RT (*1*).

Irradiated normal cells halt progression in the G_1 phase of the cell cycle by activation of p53 and pRB, which are key factors regulating cell cycle checkpoints. However, these factors are commonly inactivated in solid cancers, leading to G_1 checkpoint deficiency. Combined with oncogene-driven premature S-phase entry, this scenario evokes replication stress and enhanced chromosomal damage that requires efficient repair should the cell yield viable progenies when it divides (*2*). Hence, cancer cells particularly rely on the G_2 cell cycle checkpoint, preventing entry into mitosis with unrepaired DNA breaks (*3*). In addition, studies following the dynamics of RT-induced DNA lesions have indicated the presence of a temporally distinct and unexplained secondary wave of DNA breaks (*4*). To identify potential nuclease regulators of the G_2 cell cycle checkpoint after radiation, we screened a library targeting the known human nucleases in cancer cells (fig. S1) (*5*). The primary candidate emerging from this screen was RBBP8 (CtIP), an established DDR and G_2 checkpoint factor (*6*). Unexpectedly, a second robust target from this screen was DFFB (also known as caspase-activated DNase or CAD), a factor previously unassociated with DDR or cell cycle checkpoint control. CAD is the nuclease implicated in DNA fragmentation during apoptotic cell death as the effector of caspase signaling cascades (*7*, *8*). Caspase-mediated cleavage of CAD's chaperone and inhibitor, ICAD (inhibitor of CAD), facilitates the dimerization of CAD, giving rise to the hallmark DNA fragmentation seen in apoptosis (*8*).

CAD-inflicted DNA breaks and the ensuing DDR signals have also been implicated as inductive cues for a number of nonapoptotic cell fate states and transitions (*9*–*15*). Intriguingly, RT-induced DNA lesions encompass a temporally distinct and mechanistically unexplained secondary wave of DNA breaks (*4*). Together, these observations led us to hypothesize that CAD might be responsible for inflicting these delayed post-irradiation DNA breaks to exert checkpoint control, potentially providing a mechanism of radioresistance.

CAD promotes a wave of endogenous DNA breaks after exogenous DNA damage

To address the nature of the endogenous DNA breaks that have been reported to appear after exposure to ionizing radiation (IR), we irradiated human wild-type and CAD null (KO) colorectal cancer–derived HCT116 cells and measured the extent of DNA damage by alkaline single-cell gel electrophoresis (Comet assay) (Fig. 1A and fig. S2A). We did not observe any initial differences in DNA lesion accumulation between wild-type and CAD KO cells after exposure to IR. Further, the progressive reduction in DNA damage burden through active DNA repair was comparable between wild-type and CAD KO cells. However, consistent with recent observations (*4*), we detected a secondary accumulation of DNA lesions in wild-type cells that was prominent 24 hours after IR (Fig. 1A). The extent of DNA breakage was dependent on IR dosage (Fig. 1B). DNA break accumulation at 24 hours was largely dependent on the nuclease activity of CAD (Fig. 1C). These CAD-dependent breaks were observed in a panel of human malignant cell lines, but not in cells of nonmalignant origin (Fig. 1D and fig. S2B). To support this finding, we used in situ nick translation (ISNT) to quantify DNA breaks (*15*). This approach revealed a similar CAD-dependent elevation in DNA breaks at 24 hours after IR (Fig. 1E). CAD is normally present in a protein complex with ICAD, which also acts as a chaperone required to properly fold CAD (*8*). Accordingly, we recapitulated our observations in cells lacking ICAD, where the expression of CAD is lost (fig. S2, C and D). Further, extensive DNA DSB formation could not account for the prevalent CAD-dependent DNA breaks seen by the alkaline approach, although a discrete population of DNA DSBs might exist (fig. S2E).

PARP-1 [poly(ADP-ribose)polymerase–1] serves as a sensor of DNA lesions that triggers DNA repair and was previously implicated in the repair of DNA breaks after IR (*4*, *16*). Consistent with the appearance of DNA breaks at 24 hours after IR, we observed active ongoing DNA repair signaling, as evident from elevated poly(ADP-ribose) quantities (fig. S3A). Inhibition of PARP with 4-ANI, a strong enzymatic-activity inhibitor with only weak PARP-trapping activity, led to an elevation in DNA breaks even when the inhibitor was added for the last 2 hours of the 24-hour period after IR (fig. S3B) (*17*). The elevated PARP activity and increased DNA breaks upon PARP inhibition were both dependent on CAD (fig. S3, A and B).

The extent of single-stranded DNA (ssDNA) at 24 hours after IR was also monitored by

[1]Biotech Research and Innovation Centre, University of Copenhagen, 2200 N Copenhagen, Denmark. [2]Science for Life Laboratory, Division of Genome Biology, Department of Medical Biochemistry and Biophysics, Karolinska Institutet, 17165 Stockholm, Sweden. [3]Sprott Centre for Stem Cell Research, Ottawa Hospital Research Institute and Departments of Medicine and Cellular and Molecular Medicine, University of Ottawa, Ottawa, Ontario K1H 8L6, Canada. [4]Danish Cancer Society Research Center, 2100 Copenhagen, Denmark. [5]Institute of Molecular Genetics, Academy of Sciences of the Czech Republic, 143 00 Prague, Czech Republic. [6]Institute of Molecular Cancer Research, University of Zurich, 8057 Zurich, Switzerland.
*Corresponding author. Email: claus.storgaard@bric.ku.dk
†These authors contributed equally to this work.

Originally published 29 April 2022

native bromodeoxyuridine (BrdU) and replication protein A (RPA) foci formation. Both approaches demonstrated elevated numbers of ssDNA foci in the control irradiated cells but not in cells deficient for CAD/ICAD at this time point (fig. S3, C to H). In support of this observation, RPA foci formation at 24 hours could be restored by transient expression of wild-type CAD but not a nuclease-dead (ND) CAD variant (fig. S3I).

We postulated that elevation of DNA break quantities could signal a delayed chromatin response after IR. Consistent with this hypothesis, the maintenance of KAP1 phosphorylation, a chromatin marker of ongoing DDR, was dependent on CAD (fig. S4, A to C) (*18*). In addition to IR, we have observed a similar CAD-dependent signaling after doxorubicin-induced genotoxic damage, which also inflicts DNA DSBs (fig. S4, D to F). Collectively, these observations suggest that CAD nuclease induces self-inflicted DNA breaks in cancer cells. Canonically, caspase-3–mediated cleavage of ICAD releases CAD from inhibition, allowing for CAD dimerization. This positions each nuclease cleft in parallel across a DNA double-strand segment. Each nuclease cleft creates a single-stranded break in DNA that together produce a DSB (*8*). Notably, CAD can also inflict DNA nicks during early apoptosis and skeletal muscle differentiation (*19*, *20*). However, it has been reported that IR exposure of solid tumor cells does not elicit a robust caspase response (*21*). Here, we did not observe evidence of caspase-3 activation or proteolytic processing of ICAD after IR. Further, inhibition of pan-caspase activity did not affect the observed induction of DNA breaks, suggesting a noncanonical activation of CAD after IR (fig. S4, C, G, H, and I).

Chromatin recruitment of CAD and ICAD

We observed that both CAD and ICAD were recruited to the chromatin fraction of IR-treated cells (Fig. 2A and fig. S5A). ICAD interaction with CAD typically limits recruitment of the nuclease to DNA (*22*). However, the nuclease cleft of CAD is exposed in the CAD/ICAD heterodimer; thus, chromatin interactions could produce DNA nicks (*22*). To address whether chromatin recruitment of CAD/ICAD was sufficient to induce DNA breaks, we used the chromatin tethering model of U2OS 263 cells that harbors an integrated LacO array (*23*). Expressed mCherry-LacR-ICAD was correctly recruited to the LacO array and could recruit a green fluorescent protein (GFP)–tagged CAD to this site (fig. S5B). Analysis of the mCherry-LacR-ICAD tethered arrays in comparison to the empty mCherry-LacR construct revealed an induction of DNA breaks, as characterized by the creation of 3′-OH DNA ends that could be readily detected by terminal deoxynucleotidyl transferase end labeling

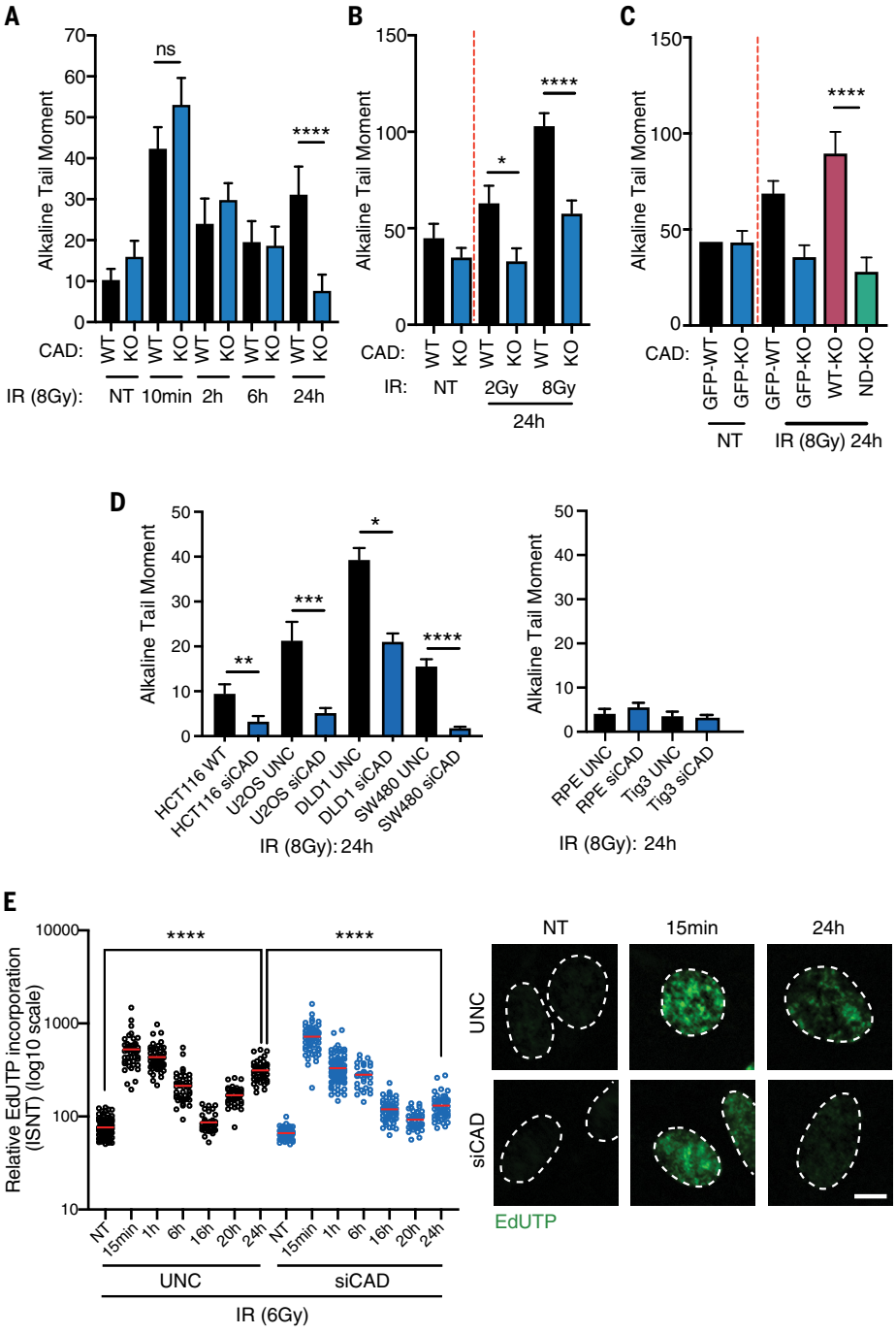

Fig. 1. CAD promotes self-inflicted DNA breaks after IR. (**A**) Alkaline Comet assay of HCT116 wild-type (WT) and CAD KO cells upon 8 Gy of IR; a representative dataset is presented. Data are means ± SEM; $N = 3$, $n > 100$. ****$P < 0.0001$ (Kruskal-Wallis multiple-comparisons test); ns, not significant. (**B**) Alkaline Comet assay of HCT116 WT and CAD KO cells upon 2 or 8 Gy of IR; a representative dataset is presented. Data are means ± SEM; $N = 3$, $n > 100$. *$P = 0.0147$, ****$P < 0.0001$ (Kruskal-Wallis multiple-comparisons test). (**C**) WT CAD, but not a ND CAD, restores DNA breaks as measured by the Alkaline Comet assay 24 hours after 8 Gy of IR; a representative dataset is presented. Data are means ± SEM; $N = 3$, $n > 100$. ****$P < 0.0001$ (Kruskal-Wallis multiple-comparisons test). (**D**) DNA break quantities 24 hours after 8 Gy of IR in cancer cell lines HCT116, U2OS, DLD-1, and SW480 and in noncancer cell lines RPE1 and Tig3 in control (UNC) or CAD-depleted cells (siCAD); a representative dataset is presented. Data are means ± SEM; $N = 3$, $n > 100$. *$P = 0.0337$, **$P = 0.074$, ***$P = 0.0001$, ****$P < 0.0001$ (Kruskal-Wallis multiple-comparisons test). (**E**) Relative ethynyl–deoxyuridine triphosphate incorporation into DNA breaks using ISNT in U2OS (control or CAD-depleted) cells upon 6 Gy of IR; a representative dataset is presented. Scale bar, 10 μm. Data are means ± SEM; $N = 3$, $n > 30$. ***$P < 0.001$ (unpaired Student's t test).

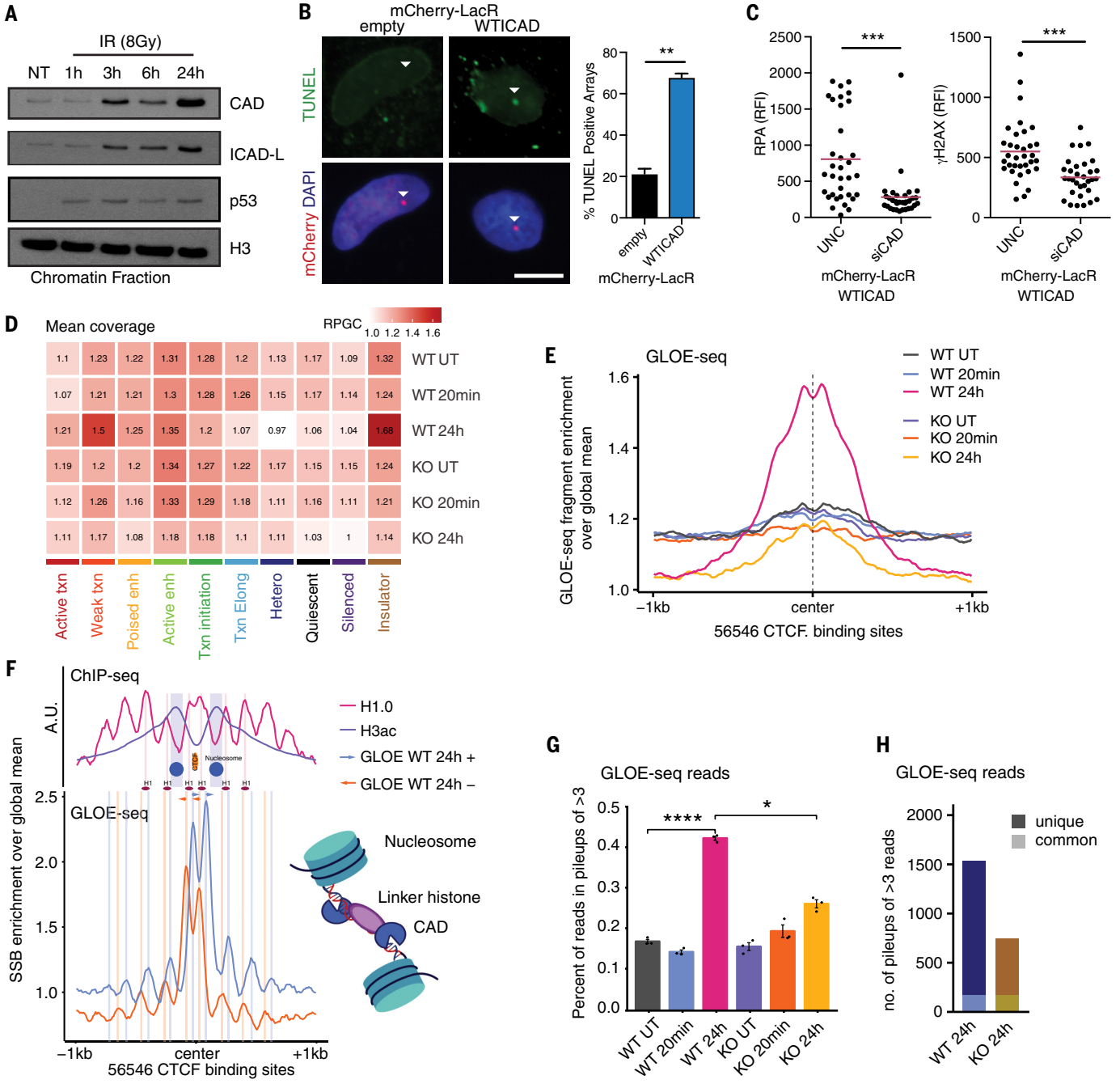

Fig. 2. CAD/ICAD chromatin recruitment inflicts DNA breaks at defined genomic elements. (**A**) Immunoblotting of chromatin fraction of HCT116 cells upon 8 Gy of IR. Recruitment of p53 was used as a positive control; H3 was used as a loading control. (**B**) TUNEL end labeling of 3′-OH indicates the formation of DNA breaks in mCherry-LacR-ICAD transfected cells. Scale bar, 10 μm. Data are means ± SEM; $N = 3$, $n > 50$. $^{**}P < 0.005$ (unpaired Student's t test). (**C**) Knockdown of CAD in mCherry-LacR-ICAD transfected cells reduces RPA and γ-H2AX. $N = 3$, $n > 20$. $^{***}P < 0.001$ (unpaired Student's t test). RFI, relative fluorescence intensity. (**D**) Genome-wide landscape of SSBs in HCT116 WT or CAD KO cells, before, 20 min after, and 24 hours after 8 Gy of IR. Average GLOE-seq read densities combined from three independent replicates are summarized over functionally distinct genomic regions as defined by a 10-state ChromHMM genome annotation. Elong, elongation; Enh, enhancer; Hetero, heterochromatin; Txn, transcription; UT, untreated. (**E**) SSB distribution around 56,546 CTCF binding sites in HCT116 cells. Average profiles from paired-end GLOE-seq fragments are plotted. (**F**) Footprint analysis of core and linker histones and SSBs around 56,546 CTCF binding sites in HCT116 cells. Linker histone H1.0 genomic occupancies are well positioned with a ~160-bp periodicity flanking the central CTCF binding site. GLOE-seq nick sites are piled up separately for the plus and minus strand. SSBs peak symmetrically and in a defined direction adjacent to the linker histone. (**G**) Three GLOE-seq replicates of each condition were filtered for duplicates and artificially over-represented regions, downsampled to the same sequencing depth (2 Mio reads), and examined for pileups of three or more unique forward reads within a 20-bp window indicating exact or near-exact coincidence of SSBs in multiple individual cells, thus "hypersensitive" nick sites. Data are means ± SEM. $^{*}P = 0.011$, $^{****}P = 5.6 \times 10^{-5}$ (Student's t test and Bonferroni correction). (**H**) A comprehensive list of pileups was generated from pooled replicates. Each pileup region was matched against the pileup regions of the other five conditions to exclude common treatment-independent hypersensitive nick sites. WT cells showed more than 1000 unique hypersensitive nick sites as compared to CAD KO cells.

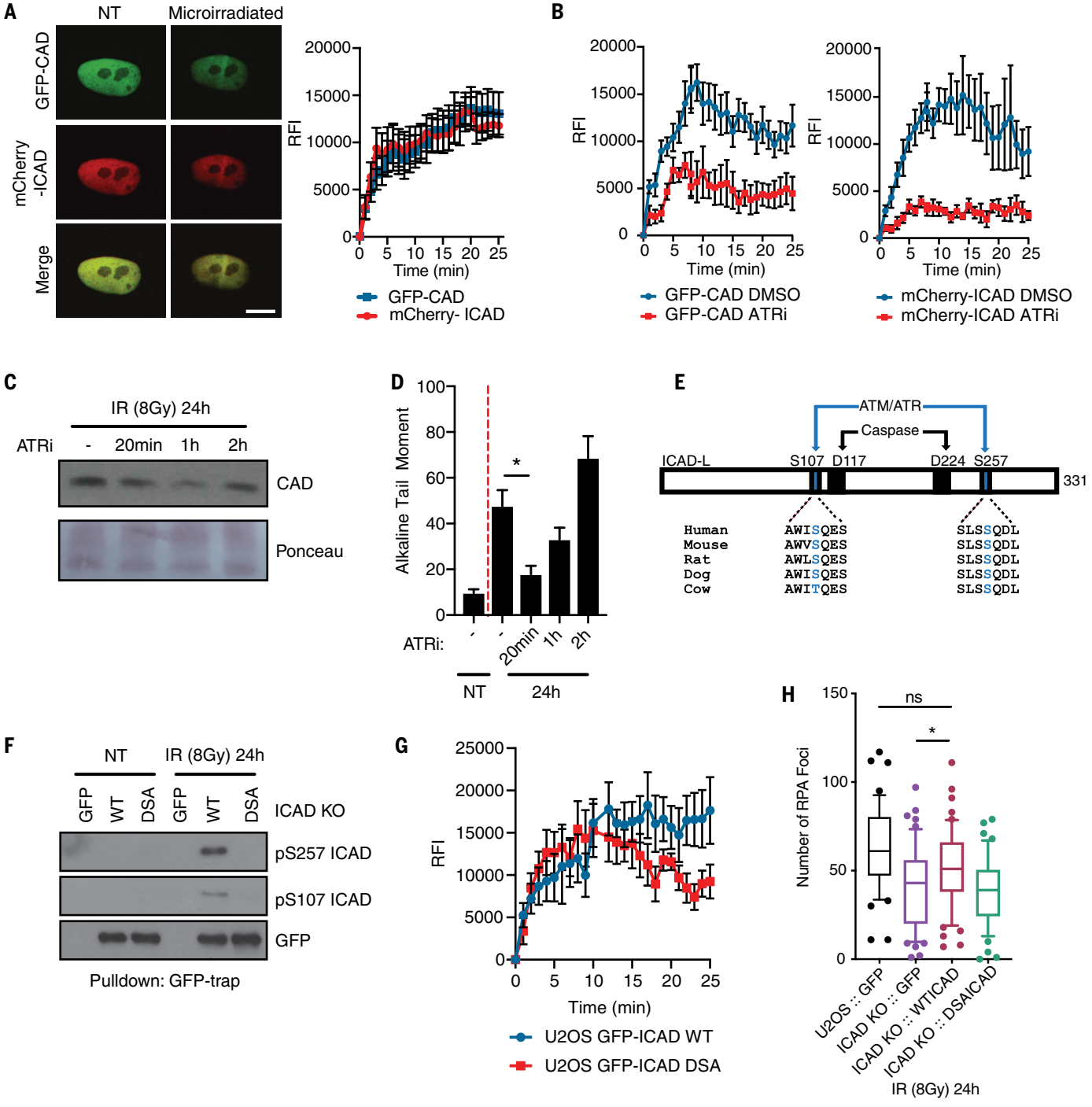

Fig. 3. ATM/ATR signaling to ICAD regulates CAD-induced DNA breaks after IR. (**A**) U2OS cells expressing mCherry-ICAD and GFP-CAD were microirradiated and imaged every minute for 25 min. Scale bar, 10 μm. Data are means ± SEM; cells per biological replicate, n = 6; biological replicates, N = 3. (**B**) Recruitment of CAD and ICAD to microirradiated laser stripes after inhibition of ATR. Conditions as in (A), except that ATRi AZ20 was added 20 min before microirradiation. RFI, SEM, replicates, and n/N are the same as in (A). (**C**) ATR inhibition (AZ20) for the indicated times prior to collection affects chromatin recruitment of CAD at 24 hours after 8 Gy of IR in HCT116 cells. (**D**) DNA break measurements under conditions like those in (C) in HCT116 cells. Data are means ± SEM; N = 3, n > 100. *P < 0.0443 (Kruskal-Wallis multiple-comparisons test). (**E**) Protein sequence analysis (Clustal Omega) of ICAD indicates two conserved ATM/ATR SQ phosphorylation motifs. (**F**) ICAD is phosphorylated at Ser^{107} and Ser^{257} after IR. ICAD KO U2OS cells expressing GFP, WT ICAD, or DSA ICAD were irradiated (8 Gy) and GFP-tagged proteins enriched by GFP trap. Immunoblotting with phospho-specific antibodies to Ser^{107} and Ser^{257} on ICAD. (**G**) DSA-ICAD is not stably recruited to laser-microirradiated damage. U2OS cells expressing GFP-WT ICAD or GFP-DSA ICAD were laser-microirradiated and imaged every minute for 25 min. Data are means ± SEM; cells per biological replicate, n = 7; biological replicates, N = 3. (**H**) RPA foci in indicated cells 24 hours after IR; N = 3, n > 50, box-and-whisker plot shows median and 10th to 90th percentiles. *P = 0.0324 [multiple-comparisons analysis of variance (ANOVA)].

(TUNEL) (Fig. 2B). Activation of the DNA damage response was noted by increased RPA association, ATR (ataxia telangiectasia and RAD3-related) association, and phosphorylation of histone variant H2AX (fig. S5, C to E). The DDR signaling from ICAD-tethered LacO arrays was dependent on CAD, as small interfering RNA (siRNA)–mediated knockdown of CAD reduced the recruitment of RPA and the phosphorylation of H2AX (Fig. 2C). Inhibition of caspase activity had no apparent effect on the recruitment of RPA to ICAD-tethered LacO arrays (fig. S5F). This demonstrates a capacity of CAD to mediate DNA break accumulation while associated with intact ICAD, independent of caspase signaling.

CAD-dependent DNA breaks at defined genomic loci

Together, our observations indicate that CAD-dependent DNA breaks appear to predominantly manifest as SSBs. To determine whether these breaks were occurring at defined genomic loci, we mapped SSBs at base-pair resolution in HCT116 wild-type or CAD KO cells before, 20 min after, and 24 hours after IR by GLOE-seq (genome-wide ligation of 3′-OH ends followed by sequencing, fig. S6A) (*24*). Examining natural SSB frequency as a function of different chromatin states, we found a weak prevalence of SSBs at active enhancers and transcription initiation sites, known to be associated with accessible chromatin, as well as insulators as defined by CTCF binding (Fig. 2, D and E). CTCF has multiple functions in genome biology as it assists the three-dimensional (3D) folding of chromatin by regulating the location of chromatin loops formation (*25*). This SSB distribution was also maintained immediately after irradiation and was independent of the presence of CAD enzyme (Fig. 2D). However, 24 hours after irradiation, a more distinctive distribution was observed in the presence of wild-type but not CAD KO cells: SSBs concentrated more on insulator regions while becoming relatively depleted in heterochromatic regions (Fig. 2, D and E). This shift in pattern was entirely consistent among replicates (fig. S6B). Consistent with the chromatin state analysis, we also observed a high enrichment of SSBs at and around CTCF binding sites 24 hours after irradiation, in a CAD-dependent manner (Fig. 2E).

We sought to more precisely pinpoint the SSBs around CTCF sites at base-pair resolution, using the mapping information of the first read, which identifies the exact nick ligation site and strand. Piling up nick sites around CTCF binding sites revealed a periodic pattern (Fig. 2F and fig. S7, A and B), with nicks in the plus and minus strand being separated by 185 base pairs. Nucleosomes are known to be well positioned around CTCF sites (*26*); hence, we used published acetylated histone H3 and linker histone chromatin immunoprecipitation sequencing (ChIP-seq) data to delineate the position of core and linker histones (*27*, *28*). Matching GLOE-seq with these ChIP-seq patterns revealed a consistent periodicity of core, linker histone, and SSB, with SSBs arising symmetrically left and right of the linker histone footprint (Fig. 2F). This suggested that DNA bound by the nucleosomes and linker histone DNA is protected from SSBs. The nick was introduced in a strand-specific manner, with the plus strand being nicked on the "plus" side of the linker histone, and the minus strand on the "minus" side of the linker histone; this suggests a potential role for histones (or chromatin structure in general) in directing and orienting CAD activity in a strand-specific manner.

CAD-induced SSBs appeared to be less random than naturally occurring SSBs. We noted initially that multiple unique GLOE-seq reads tended to accumulate at relatively few sites in the genome at 24 hours after irradiation, but not in any other condition. Thus, we used an unbiased approach to quantify SSB hotspots (more than three unique SSBs mapped in close proximity on the same strand). Twenty-four hours after irradiation in wild-type but not CAD KO cells, we observed a statistically significant ($P = 5.6 \times 10^{-5}$) factor of 2 increase across the three experimental replicates (Fig. 2G). A large number of the hypersensitivity sites that arose 24 hours after IR were new. We termed these CAD-dependent SSBs (CdSSBs), and they appeared to accumulate at hotspots different from those generally sensitive to occurrence of SSBs. Comparing wild-type and CAD KO cells 24 hours after irradiation, we observed 1371 unique pileups in wild-type cells, corresponding to putative CdSSBs, whereas ~581 unique pileups were present in the CAD KO but not wild-type cells (Fig. 2H). Notably, 232 of these 1371 CdSSBs overlapped with published CTCF peaks and 195 with DNase hypersensitive sites. Of the unique 581 pileups found in CAD KO cells, the overlap was only 11 and 14, respectively. In summary, genome-wide SSB mapping revealed a characteristic, unusual, CAD-dependent SSB landscape 24 hours after irradiation.

DDR signaling through ICAD coordinates CAD activity after genotoxic stress

Next, we investigated whether CAD and ICAD are embedded in the DDR signaling machinery in response to genotoxic stress. To explore this, we examined the recruitment of CAD/ICAD to stripes of microirradiated DNA in real time. Here, we observed that both ICAD and CAD were recruited with comparable kinetics to subnuclear regions of DNA breaks (Fig. 3A and movies S1 and S2). Unexpectedly, we noted that ICAD could also be recruited to chromatin after IR in the absence of CAD, which could indicate that the recruitment of CAD is mediated in part by ICAD after IR (fig. S8A). Examination of the recruitment to microirradiated DNA of a series of ICAD truncation fragments in ICAD-deficient cells indicated that all fragments could be recruited to irradiated regions. Fragments lacking the C-terminal domains of ICAD displayed a modest delay in accumulation (fig. S8, B to D). These results indicate that multiple regions of ICAD are responsible for chromatin recruitment.

Next, we examined whether a DDR signal could regulate the recruitment of CAD/ICAD to microirradiated stripes. We noted that inhibition or loss of ATM (ataxia telangiectasia mutated) and ATR kinase activity could limit the recruitment of CAD/ICAD (Fig. 3B and fig. S9, A to D). A similar role of the ATR kinase was also observed the day after IR, where ATR inhibition transiently diminished CAD chromatin recruitment as well as the corresponding number of DNA breaks (Fig. 3, C and D). To determine whether ATR regulates ICAD more directly, we analyzed the sequence of ICAD and identified two potential ATM/ATR phosphorylation sites, Ser^{107} and Ser^{257}, that are highly conserved across mammalian species (Fig. 3E). Further, the phosphorylation of Ser^{257} on ICAD was previously identified in phosphoproteome analysis of human cells exposed to IR (*29*). We assessed the propensity of ATR to phosphorylate ICAD in vitro, and demonstrated that ICAD can be directly phosphorylated by ATR, dependent on the ICAD SQ sites (fig. S9E). To further address the biological relevance of ICAD phosphorylation, we generated phospho-specific antibodies toward the Ser^{107} and Ser^{257} sites. Both sites appeared extensively phosphorylated after cell exposure to IR, and the phosphorylation was dependent on both ATM and ATR kinase activity 24 hours after IR (Fig. 3F and fig. S9, F to I). Next, we expressed a serine-to-alanine mutant form of ICAD that could not be phosphorylated (S107A and S257A; DSA) to investigate the functional relevance of these phosphorylation events (Fig. 3F and fig. S9F). Measuring recruitment to microirradiated stripes of DNA damage demonstrated that the DSA variant could not be stably recruited to these sites, unlike the wild-type ICAD (Fig. 3G). In addition, the DSA variant could not completely restore RPA foci formation at 24 hours after IR even though expression of CAD was restored (Fig. 3H and fig. S9F). This indicates that the ATR/ATM-dependent phosphorylation of ICAD functionally contributes to regulating the induction of DNA breaks and continued control of the checkpoint through CAD/ICAD after IR.

CAD is required for cell cycle checkpoint control and tumor cell survival after IR

Next, we investigated the role of CAD/ICAD-dependent maintenance of the G_2 cell cycle

checkpoint. We confirmed premature mitotic entry observed in the siRNA-based screen using individual siRNAs targeting CAD and ICAD and in the CAD-deficient KO cells (Fig. 4, A to C). This revealed that the breakdown in G_2 checkpoint control in CAD-deficient cells was most pronounced 24 hours after IR, which corresponded with our observed peak of CAD-inflicted DNA breaks (Fig. 4, B and C). To further characterize the molecular basis of the CAD/ICAD-dependent checkpoint regulation, we noted reduction of the inhibitory phosphorylation of cyclin-dependent kinase CDK1 (Tyr[15]), reduction in active checkpoint kinase CHK2, and moderate difference in

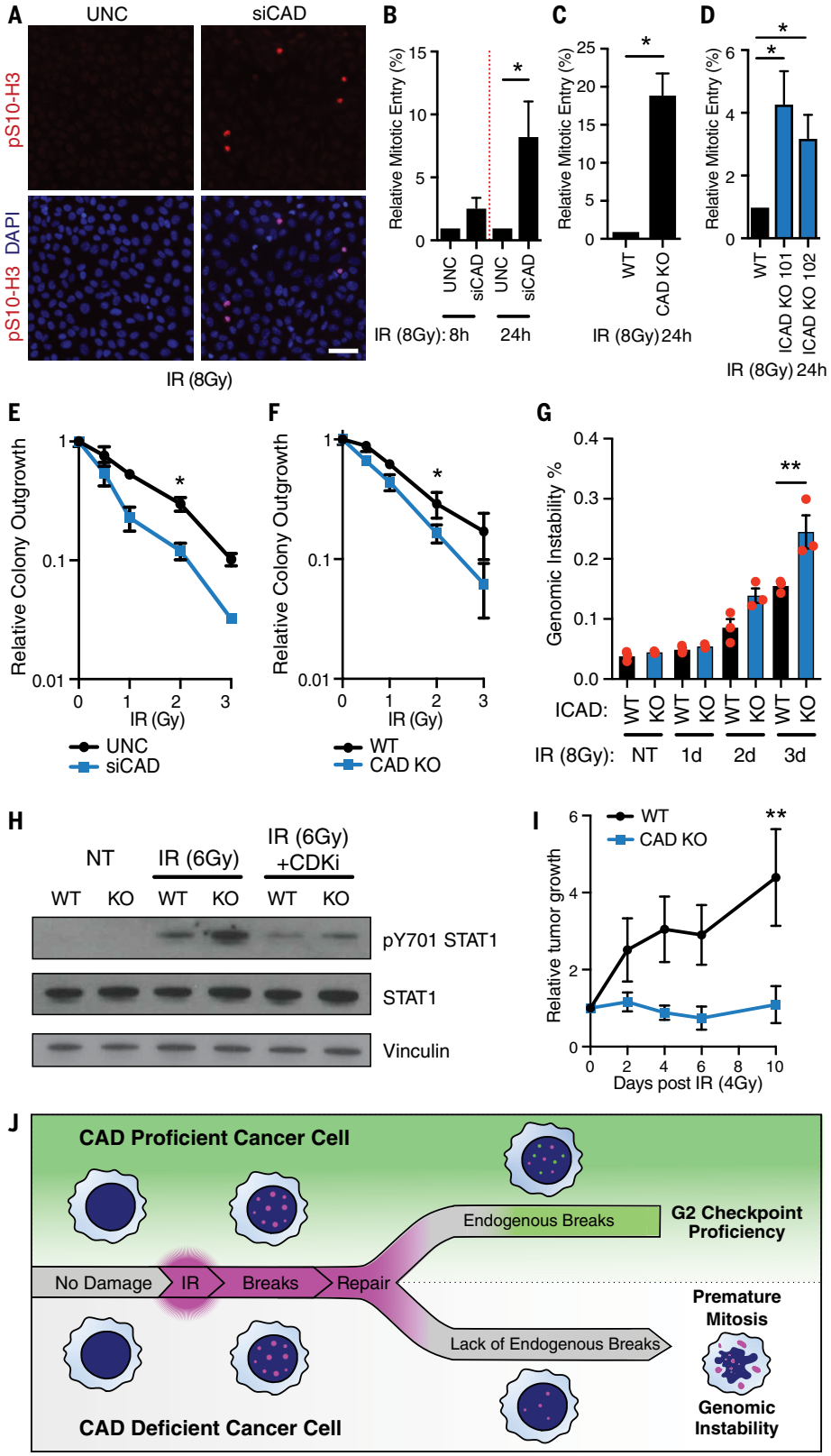

Fig. 4. CAD/ICAD are required for tumor cell survival and checkpoint maintenance after IR. (**A**) Mitotic (pS10-H3) staining of irradiated and nocodazole (NZ)–trapped U2OS cells transfected with control siRNA (UNC) and siRNA against CAD. Cells were irradiated with 6 Gy of IR; after a 2-hour recovery, NZ was added for 8 hours before cells were fixed for immunofluorescence. Scale bar, 50 μm. (**B**) G_2 checkpoint maintenance in HCT116 CAD siRNA knockdown cells upon 8 Gy of IR. Data are means ± SEM; $N = 3$. $^*P < 0.05$ (unpaired Student's t test). (**C**) G_2 checkpoint maintenance in HCT116 CAD KO cells 24 hours after 8 Gy of IR. Data are means ± SEM; $N = 3$. $^*P < 0.05$ (unpaired Student's t test). (**D**) G_2 checkpoint maintenance in U2OS ICAD KO cells 24 hours after 6 Gy of IR. Data are means ± SEM; $N = 3$. $^*P < 0.05$ (unpaired Student's t test). (**E**) Relative colony outgrowth of CAD-depleted cells after IR exposures. Data are means ± SEM; $N = 4$. $^*P < 0.05$ (unpaired Student's t test). (**F**) Relative colony outgrowth of CAD KO HCT116 cells upon indicated IR exposure. Data are means ± SEM; $N = 4$. $^*P < 0.05$ (unpaired Student's t test). (**G**) Genomic instability in U2OS WT and ICAD KO cells upon 8 Gy of IR. % Genomic instability represents total number of cells displaying micronuclei and fragmented nuclei divided by the total number of cells. Data are means ± SEM; $N = 3$, $n > 400$. $^{**}P = 0.0016$ (ANOVA). (**H**) Immunoblotting of pY701 STAT1 3 days after 6 Gy of IR in WT and ICAD KO cells. CDK1 inhibitor RO-3306 was added 2 hours after IR. (**I**) Normalized tumor growth of HCT116 WT and HCT116 CAD KO tumors after 4 Gy of IR. Data are means ± SEM; $n = 6$. $^{**}P = 0.0055$ (two-way multiple-comparisons ANOVA). (**J**) Model of CAD-dependent G_2 phase checkpoint.

active CHK1 (fig. S10, A to E). CDK1 inhibition is required to restrict mitotic entry after IR. Additionally, activated CHK2 and the phosphorylation of KAP1 have also been implicated in controlling mitotic entry of cells after IR (*30*). In line with our previous observations, this checkpoint function appeared independent from caspase signaling and unrelated to apoptotic cell death (fig. S11, A to C). Further, a CAD-promoted G_2 checkpoint was not observed in nonmalignant cells (fig. S11D), as normal cells harbor proficient p53 and pRB pathways that ensure robust G_1/S transition control and diminished G_2 checkpoint dependency. The timing of G_2 checkpoint breakdown in CAD-deficient cancer cells corresponded to the kinetics of CAD-inflicted DNA breaks, indicating that this DNA modification may functionally prevent premature mitotic entry after IR. Notably, CAD/ICAD-deficient cells that entered mitosis prematurely exhibited a high number of lagging chromosomes and chromatin bridges (fig. S11E).

Aberrant cell cycle progression and premature mitotic entry with unrepaired DSBs leads to mitotic cell death, which contributes to radiosensitivity (*21*, *31*). Indeed, cancer cells lacking the expression of CAD or ICAD displayed increased radiosensitivity (Fig. 4, E and F, and fig. S12A). This phenomenon was selective for cancer cells, as loss of CAD in nonmalignant cells had no impact (fig. S12B). Failure to repair DNA breaks through the inhibition of PARP activity has been suggested to sensitize cells to IR (*32*). Therefore, we examined whether failure to repair CAD-inflicted DNA breaks would contribute to this sensitization. We found that CAD-proficient cancer cells were sensitized to radiation by the addition of PARP inhibitor 24 hours after IR. However, PARP-inhibited CAD-deficient cells did not display any additional sensitization to IR (fig. S12C). Additionally, we noted that the loss of G_2 cell cycle checkpoint control led to the increased incidence of unstable nuclei (micronuclei and fragmented nuclei) (Fig. 4G and fig. S11E). Such genomic instability is considered to be a potent molecular pattern signal that activates inflammatory STAT1 signaling (*33*). Thus, we assessed the activating phosphorylation of STAT1 at Tyr^{701} after IR in wild-type and CAD-deficient cells. This revealed elevated p-Tyr^{701} STAT1 in CAD-deficient cells after IR, which was dependent on progression through mitosis (Fig. 4H). These observations are in line with recent research demonstrating that premature progression through mitosis after radiation promotes STAT1 signaling, and our data further indicate that CAD/ICAD limits this response (*33*, *34*).

To complement the cell-based observations, we analyzed CAD function in a model of tumor radiotherapy in vivo, using human tumor xenografts and tumor growth after radiation (Fig. 4I and fig. S12, D to F). Consistent with the cell-based survival assessment, a pronounced negative impact on tumor growth was detected after irradiation in tumors deficient in CAD, relative to their CAD-proficient counterparts. The irradiated CAD-deficient tumors demonstrated elevated p-Tyr^{701} STAT1 compared to the wild-type tumors at endpoint (fig. S12G). Collectively, these results support the concept that the CAD-dependent pathway actively promotes cancer cell survival after IR. Previous murine studies had implicated CAD as a potential tumor suppressor, which was linked to pro-apoptotic function (*10*). However, analysis of gene expression data comparing normal and malignant tissues in human cancers indicated that loss of function of CAD/ICAD is a rare event (fig. S13, A and B) (*35*). Further, elevated expression of CAD in particular was noted in multiple tumor types (fig. S13, A and B)—an observation that is consistent with a potential, as yet unidentified, tumor-supporting role for CAD.

Discussion

Together, our results unravel a DDR-mediated G_2 phase checkpoint pathway where cancer cells exposed to IR inflict reversible CAD-dependent DNA breaks including the CdSSBs. These lesions stimulate signaling responses and prevent premature mitotic entry (Fig. 4J), which enhances cancer cell survival. As repair of IR-induced DNA damage progresses, the number of highly genotoxic complex DNA DSBs declines, dropping below a threshold required to maintain the checkpoint. In turn, the induction of CAD-dependent DNA breaks signals an amplification of the DDR, further stabilizing the G_2 checkpoint and thereby providing more time for repair of the more complex, difficult-to-repair, and potentially lethal IR-induced genotoxic lesions.

The observations presented here indicate that the CAD-mediated checkpoint signal is primarily dependent on the generation of CdSSBs, a form of DNA damage characterized by rapid repair kinetics. Further, we implicate the activity of PARP-1 in the repair of CAD-mediated DNA breaks, as the addition of a nicotinamide adenine dinucleotide (NAD)–like PARP-1 inhibitor, 4-ANI, promotes DNA break formation in a CAD-dependent manner. Inhibition of PARP-1 activity has been reported to impair the G_1 checkpoint but enhance the G_2 checkpoint in irradiated cells (*36*), which may be the result of loss of PARP-1–directed repair of CdSSBs leading to increased DNA lesion burden. Furthermore, we uncovered an activating role of ICAD phosphorylation mediated by the DNA damage–induced ATM and ATR kinases. This may suggest an ongoing DNA damage–mediated feedback loop that is active until repair of complex lesions is completed, at which stage the kinase signaling declines. In this regard, we note that multiple posttranslational modification sites have been identified in ICAD (www.phosphosite.org/proteinAction.action?id=9541&showAllSites=true). These additional sites suggest that multiple signaling events may converge to regulate the CAD/ICAD checkpoint pathway.

Prior observations had established a temporally delayed secondary wave of SSBs after IR; however, the origin and functional role of these lesions have remained obscure. We identified CdSSBs as the source of these lesions, which accumulate at a subset of CTCF sites in the genome. These genomic loci may be accompanied by a moderate number of CAD-dependent stochastic lesions that escape detection because of rare targeting events within unspecified regions. Functionally, CTCF sites serve as binding domains for the CTCF protein, which regulates 3D chromosomal looping and topologically associated domains (TADs) in interphase cells (*25*). In response to positioned DSBs, chromosomal loops form in proximity to the CTCF sites, which act to sculpt the chromatin spreading of the phosphorylated histone variant γH2AX. Given that CdSSBs extend cell cycle checkpoint control, an appealing concept is that the newly formed SSBs help to enforce a chromatin response to DNA damage. This is supported by the CAD-dependent phosphorylation of KAP1, a major chromatin marker of ongoing DDR. Here, CAD nuclease activity is restricted to generate CTCF-directed SSBs after IR, which is in contrast to CAD-dependent genome-wide intranucleosomal cleavage events during apoptosis. Hence, the precision of strand break formation may be a determinant in how CAD guides cancer cell survival.

On the basis of our present study, we propose that CAD/ICAD signaling is an adaptive cancer-intrinsic mechanism to resist genotoxic stress. The apparent selectivity of this stress-tolerance pathway likely reflects multiple factors that occur in cancer but not normal cells, including defects in the p53 and pRB pathways controlling G_1/S transition, oncogene-driven premature S-phase entry, enhanced replication stress, and defective DNA repair, as well as checkpoint signaling mechanisms. The CAD/ICAD-mediated pathway may reflect adaptation to the genome-destabilizing selective pressures during tumorigenesis and contribute to therapy resistance. Such a prosurvival checkpoint pathway also reveals a cancer-selective vulnerability, thereby providing a potential avenue to enhance tumor cell radiosensitivity by targeting this G_2 cell cycle checkpoint.

REFERENCES AND NOTES

1. R. A. Sharma *et al.*, *Nat. Rev. Clin. Oncol.* **13**, 627–642 (2016).
2. T. D. Halazonetis, V. G. Gorgoulis, J. Bartek, *Science* **319**, 1352–1355 (2008).

3. M. T. Dillon, J. S. Good, K. J. Harrington, *Clin. Oncol.* **26**, 257–265 (2014).
4. A. Cieślar-Pobuda, Y. Saenko, J. Rzeszowska-Wolny, Mutat. Res. **732**,9–15 (2012).
5. D. K. Klein *et al.*, *Nat. Commun.* **6**, 5800 (2015).
6. A. N. Kousholt *et al.*, J. Cell Biol. **197**, 869–876 (2012).
7. M. Enari *et al.*, *Nature* **391**, 43–50 (1998).
8. K. Samejima, W. C. Earnshaw, *Nat. Rev. Mol. Cell Biol.* **6**, 677–688 (2005).
9. R. A. V. Bell, L. A. Megeney, *Cell Death Differ.* **24**, 1359–1368 (2017).
10. B.D.Larsen, C.S.Sørensen,FEBS J. **284**, 1160–1170 (2017).
11. J. H. Song, K. Kandasamy, M. Zemskova, Y. W. Lin, A. S. Kraft, *Cancer Res.* **71**, 506–515 (2011).
12. J. D. Orth, A. Loewer, G. Lahav, T. J. Mitchison, *Mol. Biol. Cell* **23**, 567–576 (2012).
13. X. Liu *et al.*, *Cell Res.* **27**, 764–783 (2017).
14. G. Ichim *et al.*, *Mol. Cell* **57**, 860–872 (2015).
15. B. D. Larsen *et al.*, *Proc. Natl. Acad. Sci. U.S.A.* **107**, 4230–4235 (2010).
16. J. S. Brown, B. O'Carrigan, S. P. Jackson, T. A. Yap, *Cancer Discov.* **7**, 20–37 (2017).
17. J. Murai *et al.*, *Cancer Res.* **72**, 5588–5599 (2012).
18. X. Li *et al.*, *J. Biol. Chem.* **282**, 36177–36189 (2007).
19. M. H. Al-Khalaf *et al.*, *Cell Discov.* **2**, 15041 (2016).
20. V. Iglesias-Guimarais *et al.*, *J. Biol. Chem.* **288**, 9200–9215 (2013).
21. R. G. Syljuåsen *et al.*, *Cancer Res.* **64**, 9035–9040 (2004).
22. H. Sakahira, Y. Takemura, S. Nagata, *Arch. Biochem. Biophys.* **388**, 91–99 (2001).
23. S. M. Janicki *et al.*, *Cell* **116**, 683–698 (2004).
24. A. M. Sriramachandran *et al.*, *Mol. Cell* **78**, 975–985.e7 (2020).
25. C. Arnould, G. Legube, *J. Mol. Biol.* **432**, 724–736 (2020).
26. Y. Fu, M. Sinha, C. L. Peterson, Z. Weng, *PLOS Genet.* **4**, e1000138 (2008).
27. S. Walz *et al.*, *Nature* **511**, 483–487 (2014).
28. C. M. Torres *et al.*, *Science* **353**, aaf1644 (2016).
29. S. Matsuoka *et al.*, *Science* **316**, 1160–1166 (2007).
30. H. Jaiswal *et al.*, EMBO J. **36**, 2161–2176 (2017).
31. L. Galluzzi *et al.*, *Cell Death Differ.* **25**, 486–541 (2018).
32. A. Dréan, C. J. Lord, A. Ashworth, *Crit. Rev. Oncol. Hematol.* **108**, 73–85 (2016).
33. S. M. Harding *et al.*, *Nature* **548**, 466–470 (2017).
34. J. Chen *et al.*, *Cell Rep.* **32**, 108080 (2020).
35. A. R. Cortazar *et al.*, *Cancer Res.* **78**, 6320–6328 (2018).
36. M. Masutani, T. Nozaki, K. Wakabayashi, T. Sugimura, *Biochimie* **77**, 462–465 (1995).

ACKNOWLEDGMENTS

We thank the core facilities at BRIC for assistance; the CSS laboratory for insightful comments; A. H. Lund (Biotech Research and Innovation Centre, University of Copenhagen) for HCT116 p53 KO cells; D. Spector (Cold Spring Harbor Laboratory) for U2OS 263 cells; D. Durocher (Lunenfeld-Tanenbaum Research Institute) for mCherry-LacR expression plasmid; F. Zhang (McGovern Institute, Massachusetts Institute of Technology) for pSpCas9(BB)-2A-GFP and pSpCas9(BB)-2A-GFP plasmids; W. Earnshaw (Wellcome Centre for Cell Biology, University of Edinburgh) for murine CAD/ICAD coexpression plasmid (pRHS); and B. Singers Sørensen (University of Aarhus) for discussions and cell lines used during revision. **Funding:** Supported by Danish Cancer Society grants R90-A5949 (C.S.S.), R204-A12415 (J.Be.), and R204-A12617-B153 (J.Ba.); Danish Council for Independent Research grant 4004-00621 (C.S.S.); Novo Nordisk Foundation grants NNF16OC0022358 (C.S.S.) and NNF 0060590 (J.Ba.); Canadian Institute of Health Research grant 156120 (L.A.M.); a postdoctoral grant from Independent Research Fund Denmark (B.D.L.); Czech Science Foundation grant 19-07674S and Swiss National Science Foundation grant 310030_184716 (P.J.); Swedish Research council grant VR-MH 2014-46602-117891-30, Danish National Research Foundation (project CARD) grant DNRF 125, and Grant Agency of the Czech Ministry of Health grant NU21-03-00195 (J.Ba.); The European Union's Horizon 2020 program under the Marie Sklodowska-Curie grant (agreement 722729) (G.P.); and the Karolinska Institutet SFO for Molecular Biosciences, Vetenskapsrådet Junior Researcher grant 2015-04815, and H2020 ERC Starting Grant 715024 RAPID (S.J.E.). Bioinformatics analyses were performed on resources provided by the Swedish National Infrastructure for Computing (SNIC) at Uppmax server (projects SNIC 2020/15-9, SNIC 2020/6-3 to S.J.E.).
Author contributions: Conceptualization: B.D.L., C.S.S. Methodology: B.D.L., J.Be., P.Y.K.Y., R.B., G.P., S.J.E., C.S.S. Experimental work: B.D.L., J.Be., P.Y.K.Y., R.B., G.P., V.U., J.K.A., T.T.K., S.E. Data documentation: B.D.L., J.Be., R.B., G.P., S.J.E., C.S.S. Data interpretation: B.D.L., J.Be., P.J., L.A.M., S.J.E., J.Ba., C.S.S. Funding acquisition: B.D.L., J.Be., P.J., L.A.M., S.J.E., J.Ba., C.S.S. Project administration: B.D.L., C.S.S. Supervision: B.D.L., P.J., L.A.M., S.J.E., J.Ba., C.S.S. Writing–original draft: B.D.L., J.Be., C.S.S. Writing–review and editing: B.D.L., J.Be., P.Y.K.Y., R.B., L.A.M., S.J.E., J.Ba., C.S.S. **Competing interests:** The authors declare that they have no competing interests. **Data and materials availability:** All materials are available upon request from C.S.S. All sequencing data and code are available at www.ncbi.nlm.nih.gov/geo/query/acc.cgi?acc=GSE171242 and https://doi.org/10.5281/zenodo.6386176.

SUPPLEMENTARY MATERIALS

science.org/doi/10.1126/science.abi6378 Materials and Methods
Figs. S1 to S13
Tables S1 and S2
Movies S1 and S2
References (37–44)
MDAR Reproducibility Checklist

View/request a protocol for this paper from Bio-protocol.

30 March 2021; resubmitted 4 January 2022
Accepted 30 March 2022
10.1126/science.abi6378

FORTIS
LIFE SCIENCES

TEN REASONS TO SELECT FORTIS LIFE SCIENCES FOR YOUR CUSTOM MONOCLONAL ANTIBODY PROJECT

1

YOUR PROJECT GETS A CUSTOMIZED WORKFLOW.

Our scientists invest the time to understand your exact needs, work with you to develop a strategy, and create a custom workflow to drive success for your project

2

WE DE-RISK YOUR JOURNEY.

With intelligent project milestones, you're always in the loop and in control. We build checkpoints into the process where you can evaluate data and materials and proceed as planned or course-correct if necessary.

3

WE USE RABBITS, NOT MICE.

Need an antibody that recognizes a mouse target and that you can use easily with mouse samples? That's going to be harder to get with older, mouse-based technologies. Take advantage of our state-of-the-art rabbit platform.

4

WE USE TARGET-SPECIFIC B-CELL ENRICHMENT.

Our process generates robust numbers of diverse early candidates. Enrichment increases screening efficiency, allowing for parallel counter- or co-screening with additional antigens across all candidates.

5

OUR RECOMBINANT MONOCLONAL ANTIBODIES DELIVER MORE PEACE OF MIND.

Early candidates are converted to full-length recombinant antibodies by high throughput cloning. Unlike with hybridomas, there's no need to worry about true monoclonality, variable expression, mutations, or losing your critical reagent altogether.

6

OUR RECOMBINANT ANTIBODIES ARE ENGINEERING-READY.

Need a different Fc on your monoclonal antibody? Need a Fab? Need to add a tag? We can make these and other custom modifications to individual antibodies or entire sets.

7

FIT-FOR-PURPOSE SCREENING TO FIND THE MONOCLONAL THAT WORKS FOR YOU.

Want to screen multiple recombinant candidates in your application in your hands? Want to make use of our in-house screening expertise and review the data we generate? The choice is yours.

8

WE HAVE CONTROL OVER THE ENTIRE SUPPLY CHAIN AND MAKE EVERYTHING IN-HOUSE.

From recombinant protein and peptide antigens to the final antibody preparation - including bulk supply from milligrams to grams - the entire production process and quality control take place at our facilities in the United States.

9

WE KNOW ANTIBODIES.

Ever felt like a provider didn't understand what you were asking for? At Fortis, you'll talk with passionate, experienced scientists who get it. Companies and researchers like you have trusted us for their antibodies for nearly 50 years.

10

YOUR SUCCESS IS OUR #1 GOAL.

We don't just take your order and send back a few antibodies that meet minimal criteria in our lab. Our team delivers antibodies that meet your specific needs. Your research, your business, and your reputation are too important to work with providers who cut corners.

Ready to get started? Contact us by visiting www.fortislife.com/custom-antibodies

BETHYL
A FORTIS LIFE SCIENCES COMPANY

Insights from the cutting-edge of antibody research and development

Leading industry scientists provide insights into unique applications of custom antibodies for transforming human health.

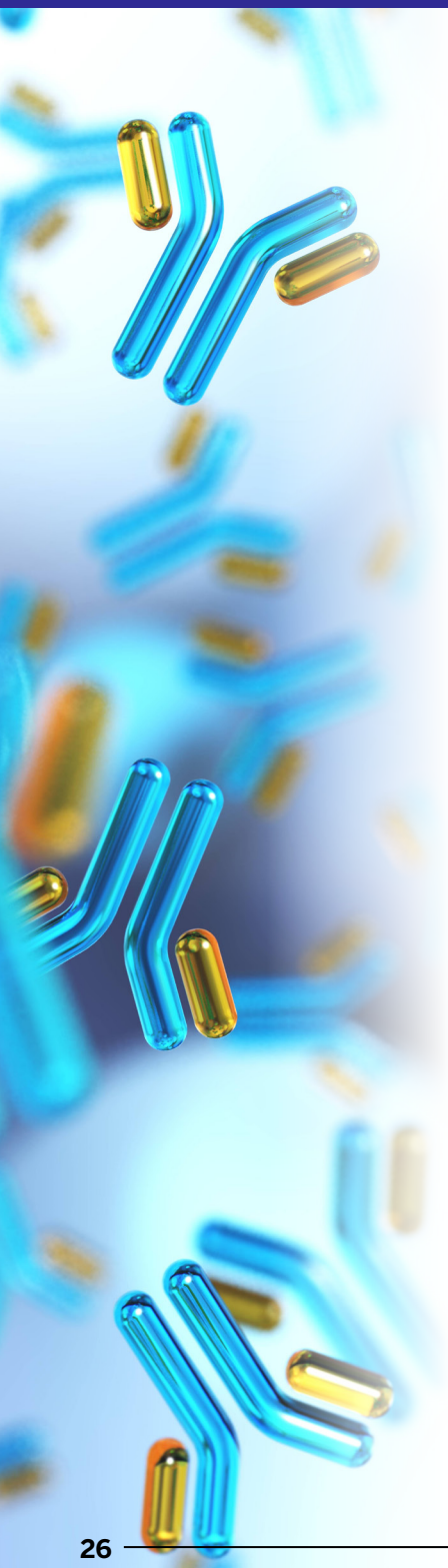

Raising the bar for biomarkers and early diagnostics in neurodegenerative disease

Lori Kobayashi
Project Manager
Valted Seq

Lori Kobayashi's diverse experience as a scientist and project manager uniquely position her to lead a research program whose goal is to identify biomarkers for early diagnosis of neurodegenerative diseases and develop diagnostic assays to monitor drug therapy. As a project manager for Valted Seq—a company using single-cell sequencing data to advance breakthrough precision therapeutics for neurodegenerative diseases—Kobayashi is using big data to break new ground.

Where has your journey as a scientist taken you?

I have a benchwork background, working at different diagnostic companies as a scientist and transitioning to project management over the last 5 years. After graduate school, I started working in a laboratory at the National Cancer Institute investigating different ways to identify natural compounds that may fight cancer, as well as screening proteins. One of those projects evolved to working with a company that was using some of the proteins we were looking at as diagnostics. So, my personal expertise is in diagnostics, with a focus at Valted Seq on neurodegenerative diseases.

What is your current research trajectory?

At Valted Seq, we are looking at novel ways to sequence brain tissue from patients who have died from Parkinson's disease in order to identify novel biomarker candidates or patterns of expression. We're also developing biomarker assays for the early diagnosis of Parkinson's disease as well as a companion diagnostic assay to monitor Parkinson's drug treatments. The overall goal is to obtain a blood draw and use diagnostics to improve Parkinson's therapy by diagnosing earlier and predicting the effectiveness of a drug over the course of treatment.

How do you use Fortis' custom antibodies to support this work?

We use enzyme-linked immunosorbent assay (ELISA)-based assays with custom antibodies from Fortis for diagnostic detection of known and novel biomarkers. Our HiF-Seq single-cell sequencing platform will hopefully

discover novel biomarker targets. Testing for a combination of various biomarkers such as alpha-synuclein and c-Abl pathway markers may lead us to earlier diagnostics for Parkinson's. We may also use certain biomarkers to track the success of a drug candidate. We will test clinical samples before, during, and after different drug treatments and compare the results to controls to determine if a certain pattern of biomarkers is related to drug treatment response and severity of disease, and whether a specific pattern may lead to earlier diagnosis. It will likely not be a single biomarker but the combination of several different ones.

We're working with Fortis to develop our own monoclonal antibodies for these potential targets. We collaborate with them to determine what to immunize the rabbits with. After they immunize the rabbits, they screen all the B-cell supernatants, and we get the top candidates that we test to see what works in our assays. A lot of these are complicated targets, and commercially available antibodies are not available for many of them. So, we're able to get our own custom antibodies.

What are some of the pain points in the process and how are they mitigated?

When working with some companies for custom antibody generation, it is necessary to splenectomize and proceed with only one rabbit. Whereas with Fortis, they immunize multiple rabbits, and they are all screened for antibodies. Fortis performs all the screenings at the end of the immunization process and provides a distribution of the best potential candidates from all the immunized rabbits. In this way, we receive multiple options for performing our own screens. They also have proprietary antigen preparation protocols that successfully generate antibodies for targets that have been unsuccessful for us with other companies in the past.

This interview has been edited and condensed for clarity.

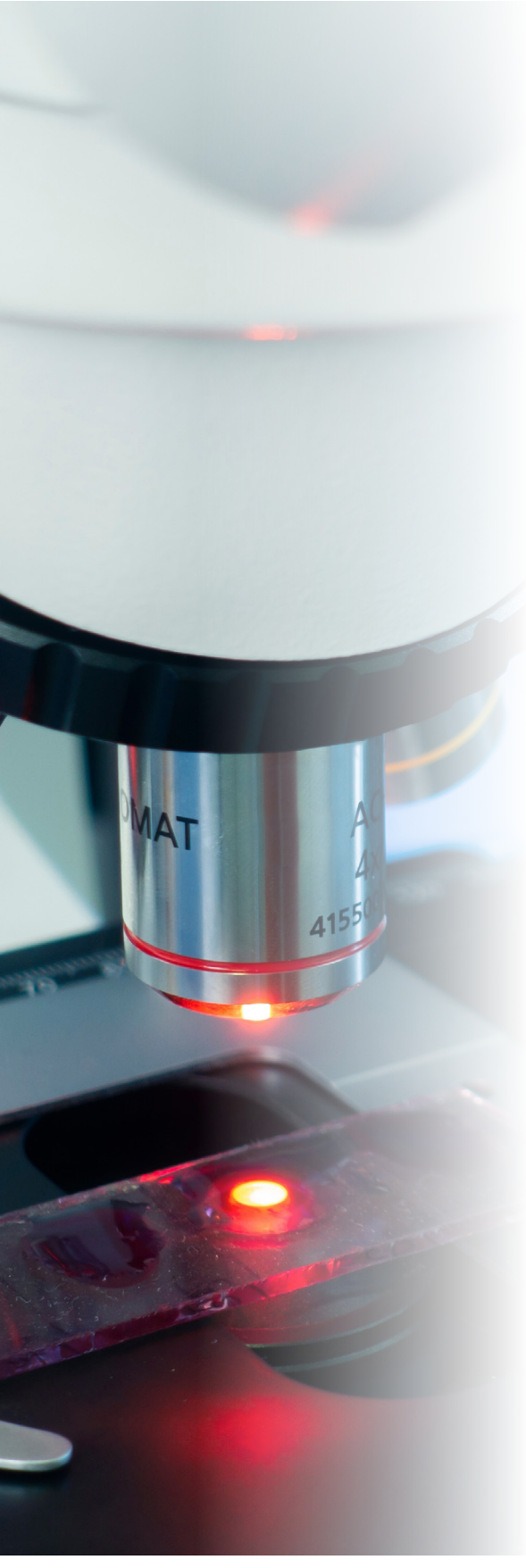

Reinvigorating the immune system to attack cancer cells using highly specific antibodies

Bijan Etemad-Gilbertson, Ph.D.
Head of Antibody Technology
NextPoint Therapeutics

Bijan Etemad-Gilbertson has over 22 years of industry experience working on antibody therapeutics for cancer at both small and large biotech companies. His expertise in manufacturing and translating antibody therapies together with his passion for scientific inquiry, drug discovery, applied therapeutics, and molecular biology drive his motivation to bring groundbreaking treatments to the clinic. In his current position as head of antibody technology at NextPoint Therapeutics, Etemad-Gilbertson leads unique R&D programs that leverage the immune system's intrinsic capacity to eradicate cancer cells.

What is the focus of NextPoint Therapeutics' innovation?

NextPoint Therapeutics is centered around a novel checkpoint axis using targeted molecules that reinvigorate the immune system to attack cancer cells. There has been a lot of success recently with PD-1, PD-L1, and CTLA-4 antibodies, which are safer and better tolerated than chemotherapy or radiation. These antibodies enter the tumor microenvironment and block immune checkpoints—proteins that normally prevent immune cells from attacking healthy cells and that are leveraged by tumors to turn off T-cell and NK-cell activity. We're blocking or derepressing these pathways.

At NextPoint, we're working on a novel pathway based on the findings of some of our founders. We're making antibody therapeutics that are highly specific to checkpoint molecules in the novel axis. We're hoping to file an investigational new drug application with the U.S. Food and Drug Administration in the first quarter of next year. As part of that we must generate a lot of assays to support the preclinical and clinical analysis. We are also generating an anti-drug activity assay to detect whether the patient's immune system makes antibodies against our molecule, which would be detrimental to the success of our drug because the immune system would clear the antibody and prevent it from working.

How are you partnering with Fortis to advance this work?

We outsource a lot of our work through contract research organizations—there are only 12 of us in the company and even though we're only three years old, we already have a huge

pipeline. We engaged with Fortis for their rabbit antibody campaign. Immunoglobulins are highly concentrated in the circulation. If an antibody is not very specific, it ends up binding a lot of things. We sent them our antibody of interest and an isotype control, which is an antibody that is exactly the same as ours except in the binding site. They immunize rabbits with our molecule, collect the B cells—which produce a very specific rabbit antibody—and screen that antibody to make sure it recognizes our molecule. They also counter screen to make sure that the positive rabbit antibody does not bind to the negative isotype control. That's a great way of finding an antibody that is incredibly specific to our drug.

This is a standard procedure with the right molecule and the right negative control. However, some molecules are not antigenic. For example, immunizing a rabbit with a molecule that is very similar to one they have previously seen may lead to tolerance and failure to generate a large immune response, in which case there may be poor antibody yield. In the past, I mostly worked with mouse monoclonal antibodies, so it was nice to see high yields with Fortis' rabbit campaign. The process was very easy because they had already cloned each B cell, so they could go back to them and then produce more antibodies to increase yields.

What are the next steps for this project?

We're going to take the lead antibodies and develop companion diagnostics. This entails working with a company that has Good Laboratory Practices and Good Manufacturing Practices facilities, which enables sending a kit to a clinical site that is ready to use.

This interview has been edited and condensed for clarity.

Setting high standards for antibody production using nucleosomes

Michael-Christopher Keogh, Ph.D.
Chief Scientific Officer
EpiCypher Inc.

Michael-Christopher Keogh's passion for epigenetics and chromatin biology helps scientists tackle complex research questions. A former academic scientist himself, Keogh is now the chief scientific officer at EpiCypher, a biotechnology company that supports transformative clinical breakthroughs across the complete cycle of innovation and commercialization—from academics engaged in fundamental explorative work to companies that deliver pioneering health innovations.

What has your journey as a scientist been like?

At the beginning, I was interested in transcription and gene expression. Everybody in the field at the time was largely working with naked DNA, a bit of genetics, and a lot of bucket biochemistry. We would all ignore the fact that transcription takes place not on a naked DNA template, but inside cells. This process is chromatinized—bundled with histones into nucleosomes. When the first transcriptional activator was definitively identified as a histone modifier [yeast Gcn5], I immediately started working on chromatin and epigenetics, and then became more broadly interested in all DNA transactions, including gene expression, damage repair, telomere maintenance, and chromosome transmission.

EpiCypher is an epigenetics and technology development company. We support academics who do early-stage research to identify new protein families and uncover the associations between mutation and disease, as well as drug developers who have already delivered multiple clinically approved drugs against different epigenetic targets. EpiCypher supports the entire ecosystem, using nucleosomes as substrates and genomic mapping controls.

What is a key research challenge that your work addresses?

One focus was to build an independent testing platform to identify whether the antibodies to histone posttranslational modifications [PTMs] that everybody was spending millions of dollars on were fit for purpose. We discovered that most are not, and in many cases even if an antibody does what it promises, there can be difficulty securing a consistent supply. Antibodies are generally developed by immunizing rabbits and are launched to the world as a single catalog number. The field has largely ignored the inherent biological variability between different lots of these reagents, even for recombinant monoclonals. We assess the performance of these reagents, demonstrating that a given anti-PTM antibody is fit for the approaches we have directly tested to nucleosome standards. We select the best-in-class to enable transformative genomic technologies, with a focus on epigenetics and chromatin. We know that antibodies are not universally capable. We are open with end users about how each antibody has been validated for a specific application, using defined and fully transparent criteria that can be independently validated.

How are you using Fortis (Bethyl) antibodies to help address this challenge?

Everybody knows how to make anti-PTM antibodies. They are a commodity developed and sold by multiple companies. But we often see profound differences in ability because these reagents are generally raised, tested, and validated to histone peptides only—the nucleosome is never considered. Bethyl has taken a different approach by implementing our tech with theirs, and what they're doing is working. Bethyl immunizes and initially screens rabbits with peptides, then exposes the candidates to our nucleosomes to determine how they deal with these chromatin subunits. Clone products are then shipped to EpiCypher for further testing to panels of PTM-defined nucleosome controls, after which the best-performing candidates are selected for scale-up and final validation in approaches of interest. EpiCypher will then release all the data that went into creating these reagents—essentially, we will show exactly what each antibody can do and will check every single lot with comparable stringency. We've been consistently pleased by Bethyl's initial candidate success rate. They are creative in their workflows, responsive to our inputs, and a great group to work with overall. We're now engaged in multiple projects, with multiple anti-PTM clones about to be launched as formal genomic mapping reagents.

This interview has been edited and condensed for clarity.

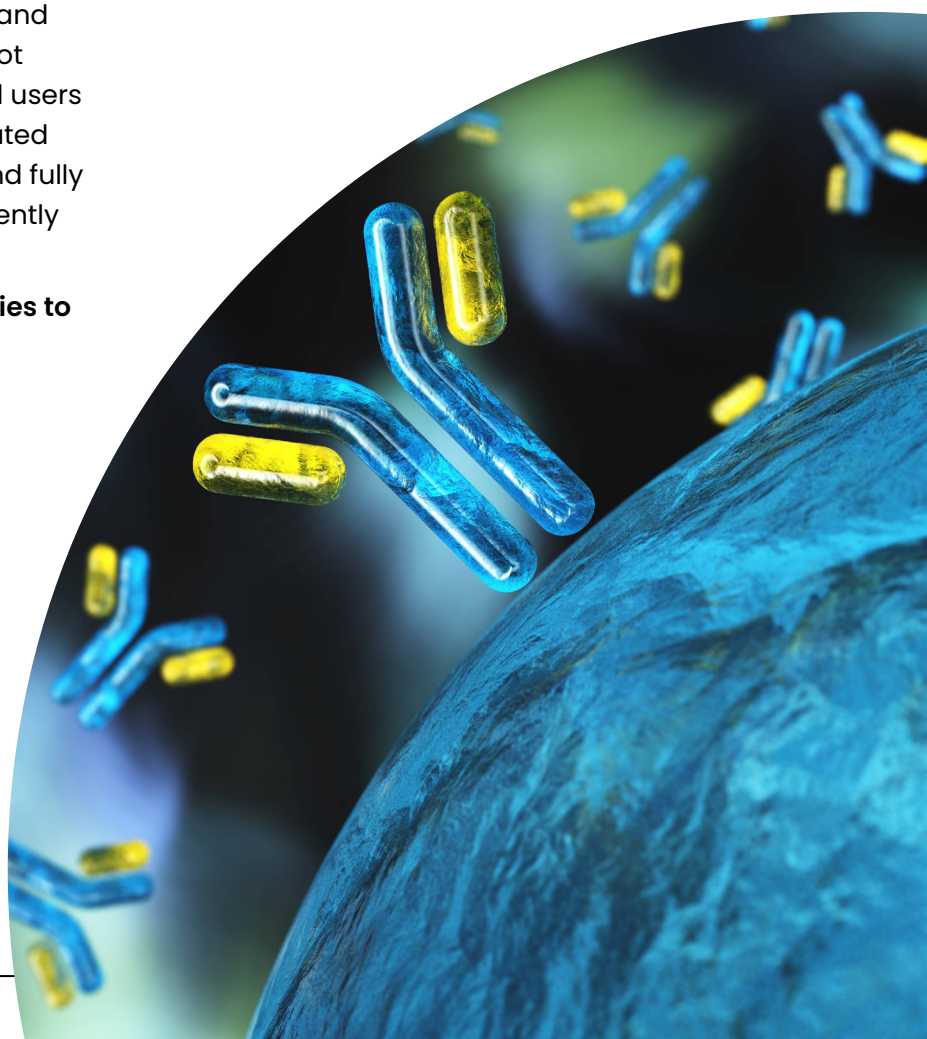

Antibody applications across science and medicine

Scientists use recombinant monoclonal antibodies to develop a broad range of research and clinical tools

For scientists seeking to create antibodies for specific applications, it comes down to one thing: choice. In a webinar titled "Recombinant monoclonal antibodies: Versatile tools for research, diagnostics, and disease therapy," David Potter—Senior Director, New Product R&D at Fortis Life Sciences, a life sciences reagent company based in Waltham, Massachusetts—explores the properties of polyclonal and monoclonal antibodies, how they can be developed, and how they can be used.

Potter describes an antibody as a wrench: "You have the business end of the wrench, which fits whatever it is designed to fit, and a handle." The variable domains in the business end of an antibody provide a diverse range of specificities that can be built into antibodies. An antibody can even distinguish between proteins that differ by a single amino acid. The handle allows antibodies to be purified through common methods of enrichment. Additionally, the constant domains of the handle can detect secondary antibodies or be used as sites for conjugation with a drug for a targeted treatment.

The two basic pieces of antibodies provide the basis for making tools for research and clinical applications, including diagnostics and therapies for a broad range of diseases, such as cancer and COVID-19. As Potter says, "We can have antibodies raised against pretty much any protein."

Polyclonal and monoclonal antibody distinctions

In general, antibodies used in research and clinical applications come in two forms: polyclonal and monoclonal. Traditionally, the development of either type of antibody starts with immunizing an animal to elicit an immune response that produces polyclonal antibodies, which can be isolated from serum or plasma. Producing monoclonal antibodies begins with cells from the immunized animal's blood or immune organs, such as the spleen or lymph nodes, and genetic material from B cells is used to make the desired antibody. Ideally, an antibody for research or clinical applications meets many criteria including specificity, unlimited and scalable production, the ability to be engineered, and minimal use of animals.

Monoclonals meet more of the desired criteria, but these antibodies cost more to produce. In some cases, polyclonals provide desirable and broader specificity. For example, a polyclonal can detect multiple areas of the target protein, which can produce a higher signal for detection. Multiple monoclonals must be used to detect this breadth of targets. Nonetheless, the nonspecific binding of a polyclonal can tag unwanted targets, which can't always be resolved. Conversely, a panel of monoclonals can be screened to tag all desired targets while eliminating off-target effects. So, the average behavior of a polyclonal comes with pros and cons, but monoclonals do not fit every research or clinical application.

Developing monoclonal antibodies

To make monoclonal antibodies, scientists can use hybridoma technology. Here, a B cell that manufactures the desired monoclonal is fused with a myeloma cell to make a hybridoma, an immortal cell line that produces the monoclonal.

Recombinant technology can also be used to make a monoclonal antibody. In general, DNA sequences for the light and heavy chains of an antibody are transfected into a cell line such as Chinese hamster ovary (CHO) or human embryonic kidney (HEK) that then produces the desired monoclonal, which is a recombinant antibody. The DNA can be collected in three general ways: from a single B cell; through phage display applied to a collection of cells, such as peripheral blood mononuclear cells; or by sequencing the amino acids of the desired antibody and using that to engineer its DNA sequence, which Potter calls a reverse recombinant approach.

In considering these methods of making monoclonal antibodies, Potter says, "They all have advantages and disadvantages." For example, the R&D cost of making hybridomas is an upside, but the time required to

make them and the limited throughput are downsides. Conversely, methods based on screening single B cells are fast and provide high throughput, but these methods are expensive. The reverse recombinant approach provides good antibody expression, but as Potter says, "It's still an expensive endeavor, and there aren't very many service providers that can perform this."

Comparing the properties

The method of manufacturing a monoclonal antibody also impacts its performance. With hybridomas, for example, Potter says, "In a perfect world, all you would have in there is a single species of hybridoma that is producing antibodies against your antigen." In practice, though, he points out that it's very common for a hybridoma to produce antibodies against the desired target and other targets. To get a pure monoclonal from this method often requires subcloning.

Recombinant antibodies avoid the hybridoma-based problems. "Recombinant antibodies start from isolated DNA for the heavy chain and the light chain, and typically those are maintained in bacteria where it is possible to pick a single colony for each chain and to confirm by sequencing that what you're looking at is a single desired sequence," Potter says.

In all cases, scientists want monoclonal antibodies to be available on demand. With monoclonals made from hybridomas, this is mostly the case, but it takes some work to maintain the frozen stock. Plus, hybridomas don't always expand predictably, and a hybridoma can produce different levels of an antibody over time. Nonetheless, Potter notes, "Hybridoma-derived antibodies are very well established in the diagnostic space." He says that about 80% of approved therapeutic antibodies were developed from hybridomas.

Recombinant monoclonal antibodies have some advantages compared to hybridomas, especially when it comes to clinical applications. When a recombinant antibody is needed in large scale, it can be incorporated in a stable cell line such as in CHO, which is expensive and can take 3–6 months. Once a CHO cell line is created, however, the track record of using this technology to produce drugs provides some regulatory acceptance. This method of making monoclonals via recombinant technology is also gaining traction in the diagnostic market. For all applications, recombinant technologies allow antibody engineering, which is not possible with hybridomas. Potter emphasizes that one benefit of antibody engineering is humanization, which converts a mouse monoclonal antibody to a minimally immunogenic human monoclonal. And for recombinant monoclonals, while some physical material such as a plasmid is stored, Potter also points out that a scientist also has the sequence, which can be saved and used essentially forever.

Although Potter noted that "the founding species in monoclonal antibody technology was the mouse," he discussed other mammalian models. For example, the larger size of rabbits makes them more useful than mice in producing polyclonals. In addition, Potter pointed out that camelids (camels, llamas, and alpacas), which produce antibodies with only a heavy chain, are ideal for phage display and engineered antibodies, such as bispecific antibodies that can bind two targets.

Despite the benefits of making antibodies with animals, Potter notes the desire to use as few as possible. Still, he added that "while animal usage can be eliminated from production with recombinant monoclonals, I would argue that we've yet to develop the technology that truly matches the antibody development, power, and efficiency of an intact immune system," meaning that animals must still be used.

Choosing wisely

Potter concludes this webinar by noting that polyclonal antibodies serve an important need in research and diagnostics. For a limitless supply of a single antibody, though, researchers use monoclonals. Recombinant technology provides more flexibility and efficiency for monoclonal antibodies than it does for hybridomas. Consequently, recombinant monoclonal antibodies are "really now starting to gain traction," says Potter.

FORTIS
LIFE SCIENCES

Looking for a better way to get custom antibodies?

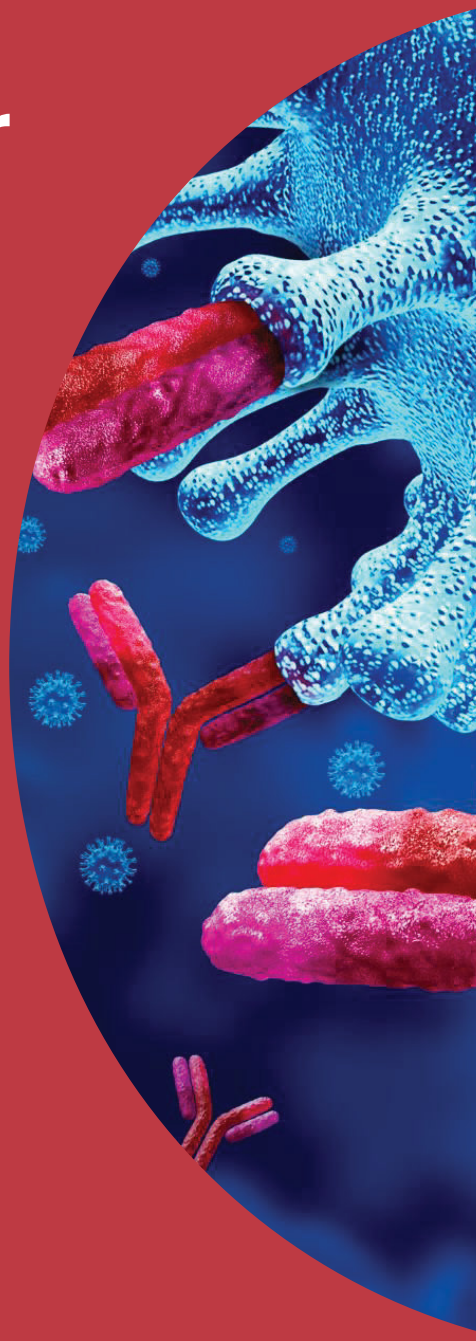

Having the right custom antibody for your application can mean the difference between a breakthrough and going back to the drawing board.

Here's just a sample of what sets us apart:

- We are 100% vertically integrated and manage the entire production and QC process at our U.S.-based facilities
- We collaborate with you to develop a custom solution to meet your scientific needs and budget
- You validate each milestone's deliverables, and we only move forward when you are completely satisfied with the progress
- We generate numerous candidates for you to test in your assays and workflows, in order to mitigate risk in the project
- Our senior scientists work closely with you and provide expertise and updates to you every step of the way

Learn more at fortislife.com/custom-antibodies

BETHYL
A FORTIS LIFE SCIENCES COMPANY

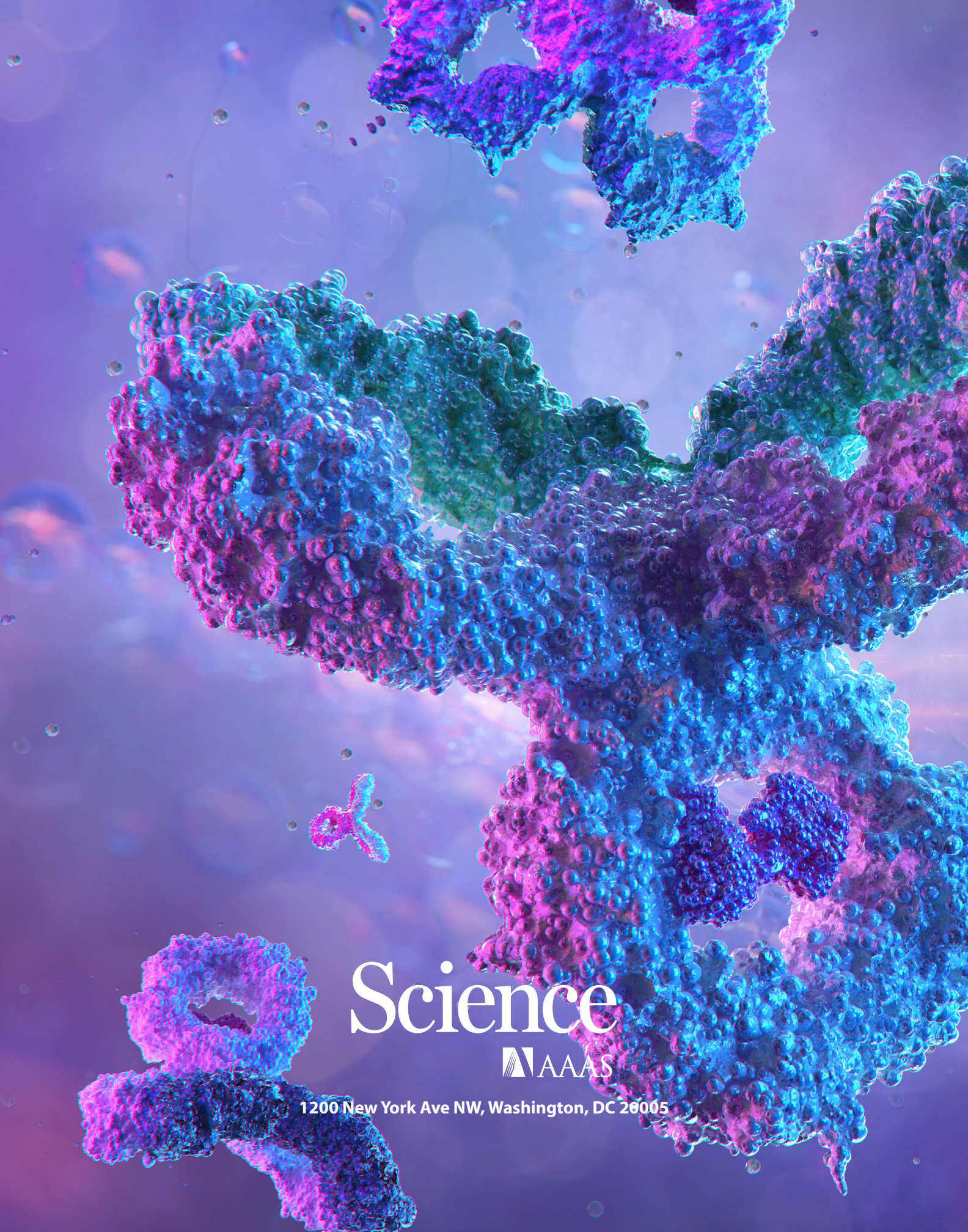
Science
AAAS
1200 New York Ave NW, Washington, DC 20005